MOLECULAR, FUNCTIONAL AND MODELING STUDY OF CYSTIC FIBROSIS TRANSMEMBRANE CONDUCTANCE REGULATOR (CFTR) MODULATION OF CHLORIDE HOMEOSTASIS IN THE RAT LUMBAR SPINAL CORD DURING POSTNATAL DEVELOPMENT

Thesis submitted for the degree of "Doctor Philosophiae"

S.I.S.S.A. – Neurobiology Sector

Candidate: Alexey Ostroumov

Supervisor: Prof. Andrea Nistri

TABLE OF CONTENTS

NOTE

During my Ph.D. years in S.I.S.S.A., I presented the following studies at the international conferences:

1. Ostroumov A., Simonetti M. & Nistri A. Developmental Regulation of the Mechanisms Controlling Chloride Homeostasis in the Rat Spinal Cord. Abstracts, the Forum of European Neuroscience (FENS 2008), Geneva, Switzerland.
2. Ostroumov A., Simonetti M. & Nistri A. CFTR controls the chloride ion homeostasis in rat spinal motoneurons during postnatal development (7th ECFS Basic Science Conference), Carcavelos, Portugal, 2010.
3. Ostroumov A., Simonetti M. & Nistri A. CFTR modulates chloride homeostasis in the developing rat spinal cord. Abstracts, the Forum of European Neuroscience (FENS 2010), Amsterdam, Netherlands.

I also submitted the paper which is under review:

1. Ostroumov A., Simonetti M. & Nistri A. Cystic Fibrosis Transmembrane Conductance Regulator (CFTR) modulates chloride homeostasis in motoneurons of the rat spinal cord during neonatal development.

All the work reported here arises solely from my own experiments, data analysis or modeling.

ACKNOWLEDGEMENTS

I would like to express my gratitude to Prof. Andrea Nistri for his careful supervising, invaluable help and support during my Ph.D. years.

I would like to thank Dr Konstantin Ostroumov for his patient teaching and useful discussions on my project.

I also wish to thank Dr Manuela Simonetti for the great help with setting up all the molecular biology experiments.

Many thanks to the people of the Neurobiology Sector for such a pleasant scientific environment and friendly atmosphere.

Thank you to all my family and friends for support and concern, which make my work and life much more nice and meaningful.

ABSTRACT

In the mature central nervous system (CNS) GABA and glycine are the major inhibitory neurotransmitters. They act via shunting incoming excitatory currents and via moving the membrane potential away from the action potential threshold. However, during development, the action of GABA or glycine can be depolarizing and become even excitatory. This phenomenon plays a significant role in the maturation of the CNS, including neuronal migration and growth, synapse formation and plasticity of GABA synapses (Ben-Ari, 2002). Since synaptic inhibition operate mainly through Cl^- fluxes, developmental regulation of this anion is crucial for the establishment of GABA/glycine inhibition.

Neuronal Cl^- homeostasis is controlled by the activity of several Cl^- cotransporters, exchangers, and channels. Basically, developmental changes in GABA/glycine signaling are determined by the opposite action of two principal cation-chloride cotransporters, namely NKCC1 and KCC2 (Payne et al., 2003). The relative contribution to Cl^- transport (uptake and extrusion, respectively) by these transporters determines the direction and magnitude of the Cl^- current through GABA or glycine channels. Ostroumov et al. (2007) reported that Cystic Fibrosis Transmembrane Conductance Regulator (CFTR) is also involved in this process in the rat lumbar spinal cord, probably through regulation of the Cl^- transporter NKCC1.

The present Ph.D. research project aimed at investigating in rat lumbar spinal cord during the first postnatal week how CFTR expression and function may change and what impact may have on inhibitory synaptic potentials in relation to KCC2 and NKCC1. This region of the spinal cord was selected since it is known to contain the central pattern generator

of locomotion (Goulding, 2009; Kiehn, 2006) that relies heavily on GABAergic and glycinergic inhition for its correct operation. Thus, with real-time RT-PCR and immunohistochemistry the gene expression and protein location of CFTR, NKCC1 and KCC2 was examined in neonatal spinal cord at various postnatal days. The Cl^- outward transporter KCC2 gene was upregulated in females over males and increased from P1 to P8. The gene activities of the Cl^- inward transporter NKCC1 and CFTR were positively correlated and grew between P1 and P8 without sex difference. P1 motoneuronal somata were immunopositive for CFTR whose expression later (P8) extended to cell processes. KCC2 immunopositivity outlined somata and cell processes at P1 and P8.

Electrophysiological recording was used to investigate the CFTR function in terms of its contribution to postnatal Cl^- regulation. Sharp electrode recording with the CFTR blocker glibenclamide showed increased motoneuron input resistance, indicating CFTR to be functional in motoneurons between P1-P8. Whole cell patch-clamping of spinal motoneurons showed that glibenclamide produced a negative shift in GABA/glycine reversal potential ($E_{GABA/Gly}$) of spontaneously occurring synaptic events measured after block of excitatory transmission. A similar effect on $E_{GABA/Gly}$ was induced by the NKCC1 inhibitor bumetanide.

Finally, a recent 3D model of the neonatal rat motoneuron (Ostroumov, 2007) was used to study the potential impact of CFTR inhibition on motoneuron excitability and $E_{GABA/Gly}$ by taking into account the age-dependent expression and distribution of this protein. Simulations suggested that CFTR activity contributes to set the $E_{GABA/Gly}$ positive to the resting potential with a depressant action on spike generation early after birth and at the end of the first postnatal week.

INTRODUCTION

There is a dynamic ratio between excitation and inhibition, which is very important for the normal function of the nervous system. The control of this ratio is partly provided by fast chemical synaptic transmission. Excitatory neurotransmitters like glutamate or acetylcholine and inhibitory neurotransmitters like GABA or glycine operate through ionotropic channels which are permeable to cations or anions respectively. Excitatory and inhibitory neurotransmission and pioneer studies on these topics are described in specialized textbooks (Eccles, 1964; McLennan, 1970)

The present study focused on investigating the impact of CFTR on the rat spinal cord Cl^- mediated inhibition produced by GABA or glycine during postnatal development. Thus, this introduction will describe the developmental establishment of GABA/glycine inhibition and the role of canonical transporters in this process in the spinal cord and other regions of the CNS. Then, the role of CFTR and its function in non-neuronal cells will be discussed. Finally, the poorly explored issue of the expression and function of CFTR in the nervous system will be reviewed.

1. INHIBITION IN THE DEVELOPING CENTRAL NERVOUS SYSTEM

1.1. GABA and glycine during development

Glycine and GABA are the major inhibitory transmitters in the adult mammalian spinal cord (Nishimaru and Kakizaki, 2009). GABA mediates most of its effects through two

classes of receptors: $GABA_A$ and $GABA_B$ receptors. While $GABA_B$ receptors operate through G proteins, $GABA_A$ receptors are ligand-gated ion channels permeable to Cl^- and HCO_3^- with a net effect that depends on the electrochemical gradient of these anions (Ben-Ari, 2007). The activation of $GABA_A$- and glycine-receptor–gated Cl^- channels results in an inward flux of Cl^- and membrane potential hyperpolarization. The inhibitory effect of these neurotransmitters therefore consists of two mechanisms. The hyperpolarization moves membrane potential away from the action potential threshold and this impairs action potential firing. Shunting inhibition is the second mechanism, through which either hyperpolarizing or depolarizing GABA/glycine receptor mediated responses reduce dendritic excitatory glutamatergic responses via a local increase in conductance across the plasma membrane and electrotonic dissipation of excitatory signals.

However, the action of GABA or glycine is often depolarizing in many brain areas during development (for review see Cherubini et al., 1991; Ben-Ari et al., 2007; Hernandes and Troncone, 2009; Stein and Nicoll, 2003) and spinal cord is not an exception (Gao and Ziskind-Conhaim, 1995; Takahashi, 1984; Wu et al., 1992; and Ziskind-Conhaim, 1998 for review). While Takahashi (1984) was investigating miniature depolarizing potentials and showed their glycinergic nature, Wu et al., (1992) showed the inhibitory action of GABA/glycine inhibitors on dorsal root-evoked potentials in embryonic motoneurons. It is noteworthy to mention that, despite the depolarizing action of GABA and glycine, Gao and Ziskind-Conhaim (1995) reported their inhibitory activity on spontaneous potentials and motoneuron excitability in the neonatal spinal cord. The indicator of the latter

phenomenon was failure of the action potential firing (evoked by the intracellular injection of small depolarizing currents) during GABA or glycine application.

The reason of this developmental phenomenon is the relatively high intracellular Cl^- concentration which leads to depolarizing action of GABA or glycine via anion efflux and loss of negative charges. So the polarity and magnitude of GABA and glycine receptor-mediated responses depend on the direction of the transmembrane current elicited by these neurotransmitters, its driving force being the difference between neuronal resting membrane potential and GABA/glycine reversal potential ($E_{GABA/Gly}$). Developmental changes are determined by the progressive negative shift in $E_{GABA/Gly}$ that in turn reflects the developmental reduction of intracellular Cl^- concentration (Fig. 1). It was shown that, in rat spinal motoneurons, a gradual shift from depolarizing to hyperpolarizing action of GABA/glycine occurs during the first postnatal week (Jean-Xavier et al., 2006). Cl^- was shown to be the main anion responsible for GABA/glycine action on immature spinal motoneurons (Cupello, 2003; Hamill et al., 1983; Wu et al., 1992). Since $E_{GABA/Gly}$ is identical to the equilibrium potential of Cl^- (E_{Cl}), this value can be used as a tool to study motoneuronal Cl^- homeostasis.

Figure 1. Relation between Cl^- reversal potential and intracellular Cl^- concentration obtained by the Nernst equation (from Ben-Ari, 2002).

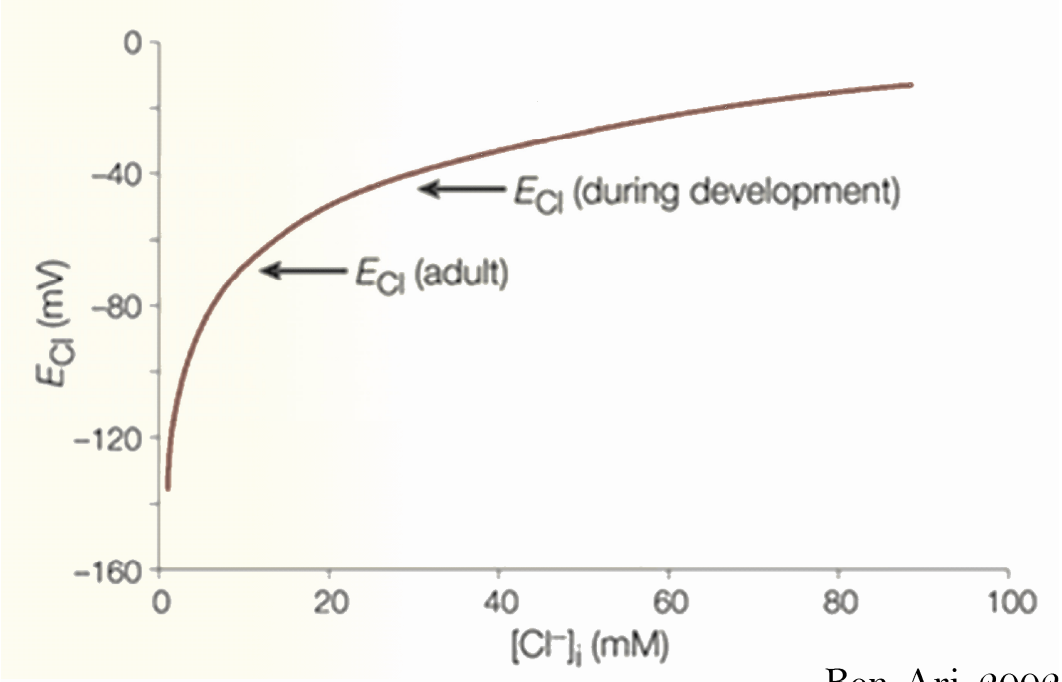

1.2. Depolarization and excitation

Despite the fact that GABA/glycine can depolarize immature neurons, the true excitatory or inhibitory nature of these depolarizations is still a matter of debate. A brief application of glycine onto the in vitro spinal cord isolated from fetal rats, at embryonic day 15.5 (i.e., 1 week before birth), evokes excitatory responses that are abolished by strychnine (Nishimaru et al., 1996). However, in the neonatal rat spinal cord it was shown that despite its depolarizing nature GABA/glycine mediated postsynaptic potential consistently inhibited synaptic excitation of lumbar motoneurons (Marchetti et al., 2002).

Therefore, there is no doubt that GABA and glycine can play an excitatory role at an early stage of the development of spinal motoneurons, but it is generally accepted that, despite their depolarizing action, GABA/glycine can already be inhibitory on neonatal spinal motoneurons because of the shunting action of the increased Cl^- conductance.

Jean-Xavier et al. (2007) demonstrated that the excitatory or inhibitory action of depolarizing inhibitory postsynaptic potentials (IPSPs) depends not only on E_{Cl} but also on location and timing of excitatory and inhibitory inputs. Using mathematical modeling and electrophysiological recording, this study showed that a suprathreshold excitatory input could be blocked by a depolarizing IPSP when the relative interval between excitatory and inhibitory synapses was short. However, when the subthreshold excitatory input was timed to occur during the decay phase of the depolarizing IPSP, then an action potential (AP) was evoked. The notion that GABA/glycine could be depolarizing and excitatory during early postnatal development has recently been challenged by the group of Zilberter (Holmgren et al., 2010; Rheims et al., 2009) suggesting that this phenomenon is the result of metabolic stress produced by the lack of adequate energy substrate during in vitro experiments with hippocampal slices. Holmgren et al. (2010) have shown that artificial cerebrospinal fluid containing glucose with other energy substrates like ketone bodies, pyruvate or lactate induces significant hyperpolarization of both membrane potential and $E_{GABA/Gly}$. Moreover, generation of giant depolarizing potentials, currently regarded as the hallmark of spontaneous neonatal network activity in vitro, is strongly inhibited in hippocampus when using the energy substrate enriched solution. Thus, such studies claim that the physiological action of GABA is always inhibitory even at birth.

1.3. Significance of GABA/glycine mediated depolarizations

The depolarizing action of GABA/glycine has been observed during early development and in several pathological conditions (Ben-Ari, 2002).

Since glutamatergic signaling operates somewhat later than GABAergic synapses, early investigations proposed that GABA should be de facto the principal excitatory transmitter during development (Ben-Ari et al., 2007). Thus, GABA/glycine mediated depolarization plays an important role in the maturation of the nervous system, including neuronal migration and growth, synapse formation and plasticity of developing GABA synapses (Ben-Ari, 2002). The first evidence that GABA may affect neurite outgrowth was provided by Eins et al. (1983). Indeed, they demonstrated that differentiated C1300 mouse neuroblastoma cells treated with GABA showed an increase in the length and branching of processes (Eins et al., 1983). Elevating intracellular Ca^{2+} concentration mediated by GABA/glycine depolarization promotes neurite length and branching not just during development, but also in adult neurogenesis (for review see Sernagor et al., 2010).

GABA/glycine play an important role in spinal nociceptive processing. The depolarizing action of these neurotransmitters at the level of the dorsal horn network is often observed during chronic pain syndromes (Coull et al., 2003; Muller et al., 2003), especially in models of spinal cord injury pain (for review see Hasbargen et al., 2010). In the cerebral cortex, the depolarizing GABA action has also been detected during epileptiform activity (Cohen et al., 2002), suggesting a contribution by weakened inhibition to neuronal hyperexcitability. A depolarizing shift in $E_{GABA/Gly}$ in response to neuronal trauma has

been observed following anoxia/ischemia, neurite transection, and osmotic imbalance (Katchman et al., 1994; Pond et al., 2006; van den Pol et al., 1996). Boulenguez et al., (2010) has recently shown that spinal cord injury caused by spinal thoracic transection in adult rats produced depolarization of E_{Cl} and, later, reduction in the strength of postsynaptic inhibition. They attributed these changes to the altered expression of cation-chloride cotransporter which maintains low intracellular Cl^- concentration in neurons. Downregulation of this transporter after spinal cord injury, particularly in motoneuron membranes, led to the disruption of Cl^- homeostasis and increased excitability of spinal networks and motoneurons (Boulenguez et al., 2010).

2. DEVELOPMENTAL CHANGES IN Cl^- HOMEOSTASIS

2.1. Cation-chloride cotransporters as regulators of Cl^- homeostasis

Developmental changes in GABA and glycine signaling are determined by the progressive negative shift in $E_{GABA/Gly}$ that in turn reflects the developmental reduction of intracellular Cl^- concentration. Neuronal Cl^- homeostasis is maintained by the functional expression of Cl^- transporters and Cl^- channels. However, the developmental shift in GABA and glycine action in hippocampus and neocortex is usually attributed to function of two cation-chloride cotransporters, namely KCC2 and NKCC1 (for review see Blaesse et al., 2009; Delpire, 2000; Payne et al., 2003). These co-transporters belong to the cation – chloride cotransporter (CCC) family. The CCC proteins are glycoproteins with estimated molecular weight of 120–200 kDa. It was suggested that all of these

transporters have a similar transmembrane topology consisting of relatively large intracellular N and C termini and a central hydrophobic domain containing 12 membrane-spanning segments (Haas and Forbush, 2000). However, the predicted secondary structure of CCCs, has so far been confirmed for NKCC1 only (Gerelsaikhan and Turner, 2000). The neuron-specific K^+-Cl^- co-transporter KCC2 is generally considered to be involved in hyperpolarizing effects of GABA and glycine and a developmental up-regulation of KCC2 expression may underlie the switch from depolarizing to hyperpolarizing responses (DeFazio et al., 2000; Rivera et al., 1999). In contrast, Na^+-K^+-Cl^- co-transporter, NKCC1, accumulates Cl^- into the cell under physiological conditions. It may therefore contribute to the high intracellular Cl^- concentration found in immature neurons (Plotkin et al., 1997b; Sun and Murali 1999). Figure 2 shows schematically how differential expression of KCC2 and NKCC1 determines developmental changes in intracellular Cl^- concentration. Recently Stil et al. (2009) investigated the expression of KCC2 and NKCC1 in the ventral horn of the rat spinal cord from the embryonic day 17 to the postnatal day 20. The significant increase in KCC2 during the first postnatal week was demonstrated and was correlated with the negative shift in the reversal potential for IPSP. Conversely, during the first postnatal week, the NKCC1 immunohistochemical signal was decreased. Co-staining experiments demonstrated that KCC2 protein is abundant in the plasma membrane of motoneurons, or in close proximity to it, whereas NKCC1 labeling was observed outside, with respect to motoneuronal somata (Stil et al., 2009). Since the specificity of the antibody used in this study is controversial (Zhang et al., 2007; Prof. Kaila, personal communication), functional experiments are necessary to investigate the role of NKCC1 in neonatal spinal cord.

Figure 2. Developmentally regulated expression of KCC2 and NKCC1 determines chloride transmembrane gradient during maturation.

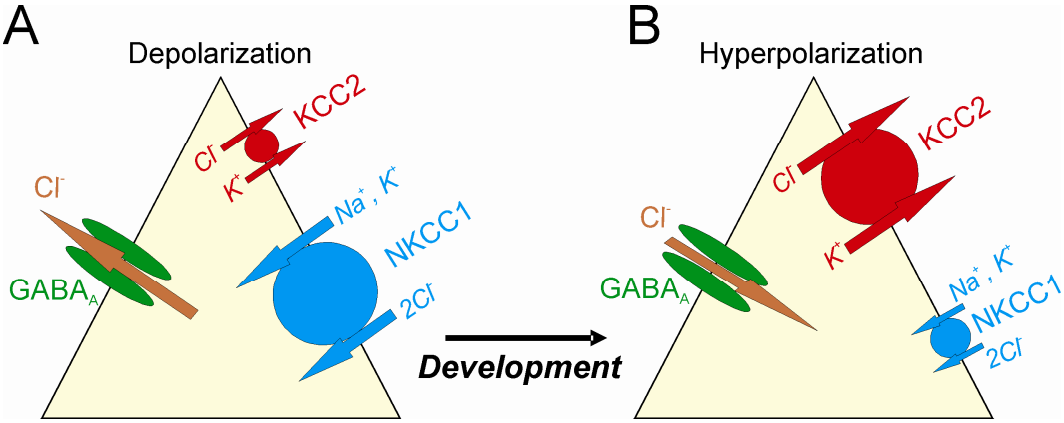

Schematic diagram depicting NKCC1, KCC2 as well as the gradients of chloride ions. A) NKCC1 expression predominates in immature neurons, in which the intracellular concentration of chloride is relatively high. B) KCC2 expression predominates in mature neurons. Note that the activation of $GABA_A$ receptors generates an efflux of Cl^- and depolarization of immature neurons, and an influx of Cl^- and an inhibition of adult neurons. Modified from Ben-Ari, 2002.

2.2. KCC2 in spinal cord and brain areas

KCC2 is an exceptional cation-chloride cotransporter as it exclusively expressed in CNS neurons (Payne et al., 1996; Rivera et al., 1999). The mammalian KCC2 (Slc12a5) gene generates two isoforms, KCC2a and KCC2b, with different N termini (Uvarov et al., 2007). The mRNA levels of the two isoforms are similar in the neonatal mouse. While the overall expression of KCC2a remains relatively constant during postnatal development, the expression of KCC2b is strongly upregulated, especially in the cortex (Uvarov et al., 2007). This indicates that KCC2b is responsible for the extensively

studied ‘‘developmental shift’’ from depolarizing to hyperpolarizing GABAergic responses. Mice that completely lack KCC2 expression die immediately after birth due to severe motor defects, including respiratory failure (Hübner et al., 2001). KCC2 is located in the plasma membrane of somata and dendrites in various brain regions including brainstem and lumbar spinal cord (Blaesse et al., 2006; Jean-Xavier, 2006), as KCC2 expression was not found in axons (Hübner et al., 2001). There is, however, a lack of drugs with a specific inhibitory action on KCC2, a fact that hampers functional studies of this transporter (Blaesse et al., 2009). The developmental increase in the expression of KCC2 parallels the shift of GABA- and glycine-evoked responses from depolarization to hyperpolarization in the hippocampus (Rivera et al., 1999; Stein et al., 2004), the neocortex (DeFazio et al., 2000) and the retina (Vu et al., 2000). In the rat auditory brainstem, KCC2 protein expression is abundant already at birth, when GABA and glycine are still depolarizing, and there is no substantial increase in KCC2 level during maturation (Balakrishnan et al., 2003). Further experiments showed that, despite this high level of expression, there was no KCC2 dependent extrusion of Cl^- at birth because the transporter becomes functional later during development (Balakrishnan et al., 2003; Blaesse et al., 2006). Functionally-inactive KCC2 has also been observed in primary cortical cultures during the first few days in vitro (Khirug et al., 2005). In the rat lumbar spinal cord, KCC2 protein expression started already at embryonic stage and increased during the first postnatal week when GABA and glycine changes their action from depolarizing to hyperpolarizing (Stil et al., 2009).

2.3. NKCC1 in spinal cord and brain areas

NKCC1 is found in nearly all cell types (for review see Russell, 2000). NKCC1 knockout animals demonstrate inner ear defects, impaired blood pressure, growth retardation and difficulties in locomotion (Delpire et al., 1999; Flagella et al., 1999). In the CNS NKCC1 is found not only in neurons, but also in glial cells, the choroid plexus and vascular endothelial cells (Mikawa et al., 2002; O'Donnell et al., 1995; Plotkin et al., 1997a). However, because of inconsistent and contradictory results, general statements about developmental changes or about the cellular and subcellular distribution of NKCC1 in CNS neurons are hardly possible. Even the widespread idea that neuronal NKCC1 expression decreases during postnatal rodent development (Plotkin et al., 1997b; Yamada et al., 2004) is challenged by data that show a developmental increase in the NKCC1 mRNA and protein levels (Clayton et al., 1998; Wang et al., 2002). The current lack of a specific NKCC1 antibody suitable for immunocytochemistry makes the situation even more complicated (Blaesse et al., 2009). However, using other techniques including specific pharmacological block with low doses of bumetanide and analysis of NKCC1 knockout mice, expression of NKCC1 was found in axons of cortical pyramidal neurons (Khirug et al., 2008). In the mouse spinal cord, NKCC1 is expressed and functions early in embryonic development when GABA produces an excitatory action (Delpy et al., 2008; Hübner et al., 2001). While NKCC1 is observed in afferent neurons after birth where it plays an important role in nociception (for review see Price et al., 2005), data concerning NKCC1 expression and function in postnatal motoneurons are currently lacking.

2.4. Other contributors to $E_{GABA/Gly}$

Some studies have reported that NKCC1 is not involved in neuronal Cl^- accumulation (Balakrishnan et al., 2003; Zhang et al., 2007) or its impact is rather limited (Gonzalez-Islas et al., 2009; Khirug et al., 2008). These findings suggest that there should be other mechanisms involved in pumping Cl^- inside immature cells. This accumulator should operate in parallel (or even in absence of NKCC1) and remains unidentified. A Na^+ independent Cl^-/HCO_3^- exchanger might be a significant contributor to the Cl^- uptake mechanisms (Gonzalez-Islas et al., 2009).

In addition to its role in neuronal Cl^- homeostasis, HCO_3^- acts as a significant carrier of depolarizing current across $GABA_A$ receptors (Kaila and Voipio, 1987). This is because neuronal pH regulation leads to a much higher intracellular level of HCO_3^- than would be expected on the basis of a passive distribution. Because the intracellular concentration of Cl^- is high in immature neurons, $E_{GABA/Gly}$ are not directly affected by the intracellular HCO_3^- concentration, while in mature neurons, the HCO_3^--mediated current component can be even larger than the one mediated by Cl^- (Kaila et al., 1993). Jean-Xavier et al. (2006) showed that the reversal potential of IPSP in the rat lumbar motoneurons was similar in HCO_3^--free and HCO_3^--containing solutions during the first postnatal week.

There are other factors which are involved in GABA/glycine developmental shift from depolarization to hyperpolarization. Kelsch et al., (2001) showed that stimulation of insulin-like growth factor I receptors intensified KCC2 mediated transport in cultured hippocampal neurons. Brain-derived neurotrophic factor (BDNF) acting via tyrosine kinase receptor also increased expression of KCC2 in mice during embryonic

development (Aguado et al., 2003). Finally, in the recent report by Ostroumov et al., (2007) it was shown that CFTR is a modulator of neuronal Cl^- homeostasis in the rat lumbar spinal cord during development, probably through regulation of NKCC1.

3. CFTR IN EPITHELIAL CELLS

3.1. CFTR: role and structure

The cystic fibrosis transmembrane conductance regulator (CFTR) is a cAMP-dependent Cl^- channel, and CFTR gene mutation has been shown to cause cystic fibrosis (CF), the leading lethal genetic disease among the Caucasian population (Hanrahan et al., 2002). CFTR is an essential component of epithelial Cl^- transport systems in many organs, including the intestine, pancreas, lungs, sweat glands, and kidneys. The predicted primary structure of this protein is shown in Fig. 3A and consists of two membrane- spanning domains, two nucleotide-binding domains, and a regulatory domain (Riordan et al., 1989). CFTR structure puts it in a family of transporter proteins called ATP-binding cassette (ABC) transporters. Several members of this family utilize the energy from ATP hydrolysis to actively transport substrates across cell membranes (Riordan, 2008). However, this protein is also known to function as an ion channel.

Figure 3. CFTR structure and function.

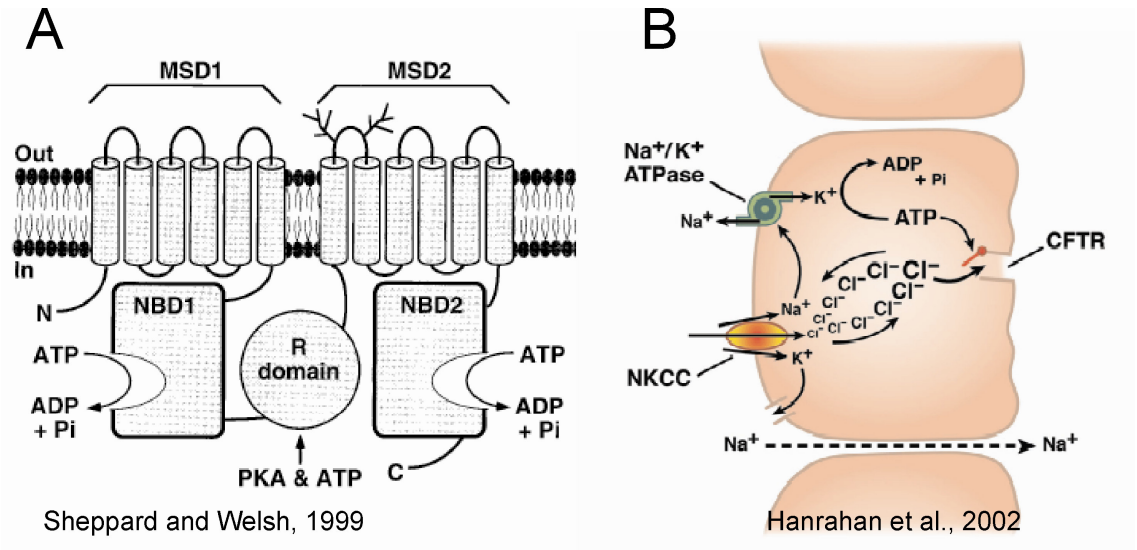

A) Model showing proposed domain structure of CFTR. MSD, membrane-spanning domain; NBD, nucleotide-binding domain; R, regulatory domain; PKA, cAMP-dependent protein kinase. From Sheppard and Welsh, 1999. B) Cross-section of the epithelium with basolateral side shown on the left and apical side on the right. Monovalent ions like Na^+, K^+ and $2Cl^-$ enter the cells from the vascular side through the NKCC1 operation. Na^+ is actively pumped out by Na^+/K^+ ATPase at the basolateral membrane, and K^+ also leaves via a basolateral potassium channel. Cl^- is raised above electrochemical equilibrium and flows to the luminal side through the CFTR chloride channel. Na^+ follows paracellularly to maintain charge balance. From Hanrahan et al., 2002.

3.2. CFTR as an ion channel

The example of Cl^- secretion in intestinal epithelial cells where CFTR acts as an ion channel is shown on figure 3B. In brief, Cl^- enters the cells through the NKCC1 cotransporter in the basolateral membrane and exits through CFTR in the apical membrane (Hanrahan et al., 2002). CFTR ion channel has a low single-channel conductance of 6-10 pS. However, there are some variations in these values depending on

recording conditions and animal species. This channel is permeable mostly to anions, namely for Cl^-, I^-, Br^- (Sheppard and Welsh, 1999). CFTR was also reported to function as a bicarbonate channel (Ishiguro et al., 2009). Water is also permeable through the CFTR channel (Hasegawa et al., 1992), whereas any ATP permeation is controversial (Reddy et al., 1996; Reisin et al., 1994). It has also been reported that CFTR is a multi-ion pore (Tabcharani et al., 1993). The sulphonylureas glibenclamide and tolbutamide were found to be CFTR inhibitors which act probably through open channel block (Sheppard and Robinson, 1997).

3.3. CFTR as a regulator of other proteins

In addition to its function as a Cl^- channel, CFTR acts as a regulator of other channels and transporters (Kunzelmann and Schreiber, 1998). CFTR mediates cAMP regulation of amiloride-sensitive Na^+ channels (Stutts et al., 1995), outward rectifying Cl^- channels (Egan et al., 1992; Gabriel et al., 1993), Cl^-/HCO_3^- exchanger (Lee et al., 1999), and the ROMK K^+ channel (McNicholas et al., 1996). Whether these regulatory functions result from direct interactions between CFTR and the channels and transporters or through indirect interactions via other proteins remains to be determined.

Shumaker and Soleimani (1999) working on a pancreatic duct epithelial cell line showed enhancement of NKCC1 expression and activity in the presence of functional CFTR. Later, Adam et al. (2005) demonstrated with cultured collecting duct cells that CFTR stimulates NKCC1 to increase intracellular Cl^- concentration.

4. CFTR IN NEURONS

4.1. CFTR expression in CNS

Originally CFTR was thought to be present in epithelial cells only (Riordan et al., 1989). However, CFTR expression in nonepithelial cells like macrophages, lymphocytes, neutrophils, and smooth muscle cells has been reported (Di et al., 2006; Fonknechten et al., 1992; Painter et al., 2006; Vandebrouck et al., 2006). Expression of this protein was also found in microglia (Liu et al., 2006) and peripheral ganglia (Niu et al., 2009). Mulberg with his associates reported expression of CFTR in neurons of different brain regions of the rat brain, including the forebrain, diencephalon, midbrain, hypothalamus and thalamus (Mulberg et al., 1994; 1995). They also reported that CFTR was associated with clathrin-coated vesicles (CCV) in neurons of the hypothalmus of the bovine brain, a finding suggesting that CFTR might be involved in neuropeptide transport or other molecular trafficking (Mulberg et al., 1994). In the human nervous system, CFTR is expressed in the anterior hypothalamus (Mulberg et al., 1998). Recently it was shown that CFTR is expressed in neuronal somata and dendrites of the human spinal cord (Guo et al., 2009). The first report of functional expression of CFTR in rat spinal motoneurons was provided by Ostroumov et al. (2007). In this study glibenclamide (50 μM) was used to study K_{ATP} channels (Mironov et al., 1998) with the help of intra- and extracellular electrophysiological recordings from lumbar spinal motoneurons and interneurons at P4-P8. But no effect of glibenclamide on rat spinal motoneurons compatible with pharmacological block of K_{ATP} channels was found. Facilitated mono- and polysynaptic

reflexes, hyperpolarized motoneuron resting potential, increased action potential amplitude, decreased Renshaw cell-mediated recurrent inhibition suggested that glibenclamide acted through CFTR inhibition (Ostroumov et al., 2007). Furthermore, this study showed that effects identical to those of glibenclamide were observed after applying tolbutamide and diphenylamine-2,2'-dicarboxylic acid (DPC), both considered to be CFTR inhibitors (Schultz et al., 1999). Finally, RT-PCR and western immunoblotting indicated strong expression of the CFTR in neonatal rat spinal cord at P4-P8 (Ostroumov et al., 2007).

4.2. CFTR function in CNS

The role of CFTR in neurons of the CNS remains unclear and the significance of its expression can be twofold. First, CFTR expression in neurons can be important for the normal function of the nervous system. Functional expression of CFTR in the hypothalamus led to the proposal that this protein might be involved in regulating energy utilization, sexual maturation, and reproductive behavior (Mulberg et al., 1995, 1998; Weyler et al., 1999). CFTR is able to mediate ATP hydrolysis, thereby regulating the flux of glutathione (GSH), which is known as a major antioxidant in the brain and neuromodulator of NMDA channels (Aoyama et al., 2008). This suggests that CFTR may profoundly affect neuronal function. Finally, this molecule can participate in the control of Cl^- homeostasis and neuronal excitability as a Cl^- channel and as a NKCC1 regulator (Ostroumov et al., 2007). This hypothesis was investigated during present Ph.D. research project.

Second, mutation or alteration of CFTR may induce CNS dysfunction in cystic fibrosis (CF). Dysfunction of CFTR in CF disrupts transepithelial ion transport and, hence, the function of a variety of organs lined by epithelia. This leads to the wide-ranging manifestations of the disease, which can include airway disease, pancreatic failure, meconium ileus, male infertility, and elevated levels of salt in sweat. Neural disorders are very rear in CF patients; however, seizures were reported in several adult CF patients (O'Mahony and FitzGerald, 1991). Lung transplant is often a life-saving treatment for CF. It is, however, interesting that those patients surviving longer after transplantation show high incidence of neurological syndromes including seizures (Goldstein et al., 2000; Quattrucci et al., 2005) perhaps compatible with dysfunction of CFTR in the central nervous system. Dystrophic axons in the nucleus gracilis and demyelination of the fasciculus gracilis have been reported in CF patients, with 66% developing dystrophic axons (Cavalier and Gambetti, 1981). Subclinical extrapyramidal hemosiderosis has also been reported in CF (Wongmongkolrit et al., 1985). Such findings cannot be explained by the pathological changes in the lungs or other organs typically associated with CF.

HYPOTHESIS AND AIMS OF THE PRESENT STUDY

Hypothesis

The present project started by testing the hypothesis that CFTR is expressed in neonatal lumbar spinal cord motoneurons where it is involved in Cl^- homeostasis through the regulation of the Cl^- transporter NKCC1.

Aims

1. Following the demonstration that the inhibitory action of GABA and glycine in the rat lumbar motoneurons strongly depends on developmental changes in intracellular Cl^- concentration during the first postnatal week, the investigation was aimed at discovering the mechanisms involved in the control of Cl- homeostasis during this period. Since NKCC1 and KCC2 were proposed as the major players responsible for the gradual shift in $E_{GABA/Gly}$ during development, the goal was to investigate age-dependent changes in expression and function of these proteins.

2. In the recent report by Ostroumov et al., (2007) it was suggested that CFTR can participate in the control of Cl^- homeostasis in rat lumbar motoneurons. So it was necessary to study expression and function of this protein during the first postnatal week. It was also important to test if CFTR could affect $E_{GABA/Gly}$ during this period. Finally, it was attempted to estimate the potential impact of CFTR on Cl^- mediated inhibition of motoneuron excitability.

METHODS

1. SPINAL CORD TISSUE PREPARATION

The spinal cord, from low cervical segment to *conus medullaris*, was isolated from neonatal Wistar rats (0 to 9 postnatal days old, P0-P9). Animals were firstly anaesthetized with an intraperitoneal injection of urethane (0.2 ml ip of a 10% wt/vol solution). As soon as the animal lost the withdrawal reflex, it was rapidly decapitated with scissors. The forelimbs and the ventral part of the chest were removed and the animal was eviscerated in order to expose the ventral side of the vertebral column. The remaining skin was also removed and the body was washed in cooled (4 °C) oxygenated (95% O_2 – 5% CO_2) artificial cerebrospinal fluid (ACSF) and fixed by pins with the ventral side up to the sylgard bottom of a Petri dish containing ACSF at the same temperature. ACSF composition was (in mM): 113 NaCl, 4.5 KCl, 1 $MgCl_2 \cdot 7H_2O$, 2 $CaCl_2$, 1 NaH_2PO_4, 25 $NaHCO_3$ and 11 glucose; pH 7.4 at room temperature. The solution contained in the dish was continuously oxygenated. A complete laminectomy was performed in the rostrocaudal direction under the microscope. Meningeal tissue was removed from the ventral side while dorsal roots (DR) and ventral roots (VR) were cut as close as possible to the dorsal root ganglia. Remaining meningeal tissue present on the dorsal side of the spinal cord was also removed. For motoneuron electrophysiological studies the spinal cord was hemisected sagitally.

2. REAL TIME RT PCR

2.1 RNA extraction

Total RNA was isolated from rat lumbar spinal cord at P1, P4, P6 and P8 following the Invitrogen protocol based on Trizol extraction. Namely, the lumbar region from L1 to L6 segments was isolated and put in 1ml of Trizol (Invitrogen), where it was homogenized and left for 5 min. 200 µl of Chloroform was added to the sample which was centrifuged for 15 min at 12000 rpm at 4 °C. Then the supernatant was collected and left for 10 min in 500 µl of isopropanol at room temperature. After centrifugation for 10 min (12000 rpm) at 4 °C all the supernatant was removed and 1 ml of ethanol (70%, 4 °C) added. Further centrifugation was applied for 7 min (7500 rpm) at 4 °C. All the supernatant was carefully removed and the pellet was resuspended in 10 µl of water. The RNA samples were kept at -80 °C until use.

2.2 Reverse transcriptase

1 µl of DNAse and buffer 10x (both Invitrogen) were added to 8 µl of RNA and left for 15 min at room temperature. Then 1 µl of EDTA (25 mM) was added and left for 5 min at 65 °C to destroy genomic DNA. To 8 µl of RNA, 1 µl of dNTP, 0.5 µl of oligo-dT and 0.5 µl of random hexamers were added. After 5 min at 65 °C the following reagents were subsequently added: 2 µl of RT buffer, 4 µl of $MgCl_2$ (25 mM), 2 µl of DTT (0.1 M), 1 µl of RNase OUT (40 u/µl) and 1 µl of SuperScript III RT (200 u/µl). All the oligos were

from Invitrogen. Solutions were kept for 10 min at room temperature, 50 min at 50 °C and, finally, 5 min at 85 °C. cDNA was kept at -20 °C.

2.3 RT PCR

Quantitative PCR was performed in a Bio-Rad (Hercules, CA) iQ5 thermocycler using IQ SyBr Green Supermix. Reactions were performed in the presence of specific primers for CFTR, NKCC1, and KCC2 (Table 1). Data normalization was carried out with respect to glyceraldehyde-3-phosphate dehydrogenase (GAPDH) and neuronal β-tubulin III housekeeping mRNA content.

Solutions with SyBr Green were prepared for each pair of primers (contents in µl: 25 SyBr Green Supermix, 1 forward primer, 1 rewind primer, 18 H_2O). First cDNA was dissolved two times and then subsequently 1:5 and 1:25 to create a standard curve. cDNA was mixed with SyBr Green solution and put in a PCR well plate in duplicate for each sample. Negative controls containing no template cDNA were run with each pair of primers in each condition and gave no result. To ensure absence of amplification artifacts, end point PCR products were initially assessed on agarose gels that gave a single band of the expected size for each primer.

2.4 Data analysis

Analysis was performed using the $2^{-\Delta\Delta CT}$ method (Livak and Schmittgen, 2001).

The reactions were quantified when the PCR product of interest was first detected (cycle threshold). Calculations for relative mRNA transcript levels were performed using the comparative C_T method ($\Delta\Delta C_T$) between cycle thresholds of different reactions (Livak and Schmittgen, 2001). In particular, for age dependent gene expression changes, the parameter C_T (threshold cycle) was defined as the cycle number at which the fluorescence emission exceeds the fixed threshold. The calculation was based on the difference (ΔC_T) between the C_T values of the target (CFTR, NKCC1, KCC2) and the housekeeping genes (GAPDH or β-tubulinIII) at each time-point at different ages, and then normalized with respect to the ΔC_T value of the P1 sample. For sex difference experiments, normalization was made with respect to the male signal.

2.5 Laser capture microdissection

To investigate gene expression in distinct cell types, laser-capture experiments were performed. The laser pressure catapulting technique allows isolating in a plastic cap only one individual cell. Lumbar segments of spinal cords at P1 and P8 were frozen in liquid nitrogen and sectioned at 16 µm with a cryomicrotome. To distinguish motoneurons from other cell types slices were incubated for 15 minutes in 1% cresyl-violet dissolved in RNase free water. I then used a Zeiss PALM system (Carl Zeiss Microimaging) to image, cut and catapult motoneurons. Criteria for motoneuron selection included localization in the ventral part of the spinal cord; a diameter of at least 20 µm and an identifiable nucleus (Perrin et al., 2006; Fig. 4).

RNA was isolated from cells following The Absolutely RNA Nanoprep Kit protocol (Agilent technology). Briefly, isolated cells were homogenized and protected from RNases using a mixture of β-mercaptoethanol, lysis buffer and ethanol (70%). After serial usage of High- and Low-Salt Wash Buffer, RNA was stored at -80 °C.

RNA was retrotranscribed and real time RT PCR was performed as described above. I used an astrocytic marker S100B (Kuzhandaivel et al., 2010; Wang and Bordey, 2008; Table 1) to test if motoneurons were the only cell type I was collecting.

Table 1. Primers used for real time RT-PCR experiments.

	Primer sequence	Tm (°C)
CFTR	Fw: 5'-GGCAATGTCTGGCAGTATGAATC-3' Rw: 5'-GCACTTCTTCCTCCGTCTCC-3'	58
NKCC1	Fw: 5'-TGGTCACATACACTGCCGAAAG-3' Rw: 5'-TCCTCCTCCTCTCACGAATCC-3'	59
KCC2	Fw: 5'-CACCTACGAGAAGACATTGG-3' Rw: 5'-CGAGTGTTGGCTGGATTC-3'	54
β-tubulin III	Fw: 5'-CGCCTTTGGACACCTATTC-3' Rw: 5'-TACTCCTCACGCACCTTG-3'	55
GAPDH	Fw: 5'-CAAGTTCAACGGCACAGTCAAG-3' Rw: 5'-ACATACTCAGCACCAGCATCAC-3'	60
S100B	Fw: 5'-TCCACACCCAGTCCTCTC-3' Rw: 5'-GCTTGTCACCCTCTCTCC-3'	58

Figure 4. Laser-capture microdissection experiments.

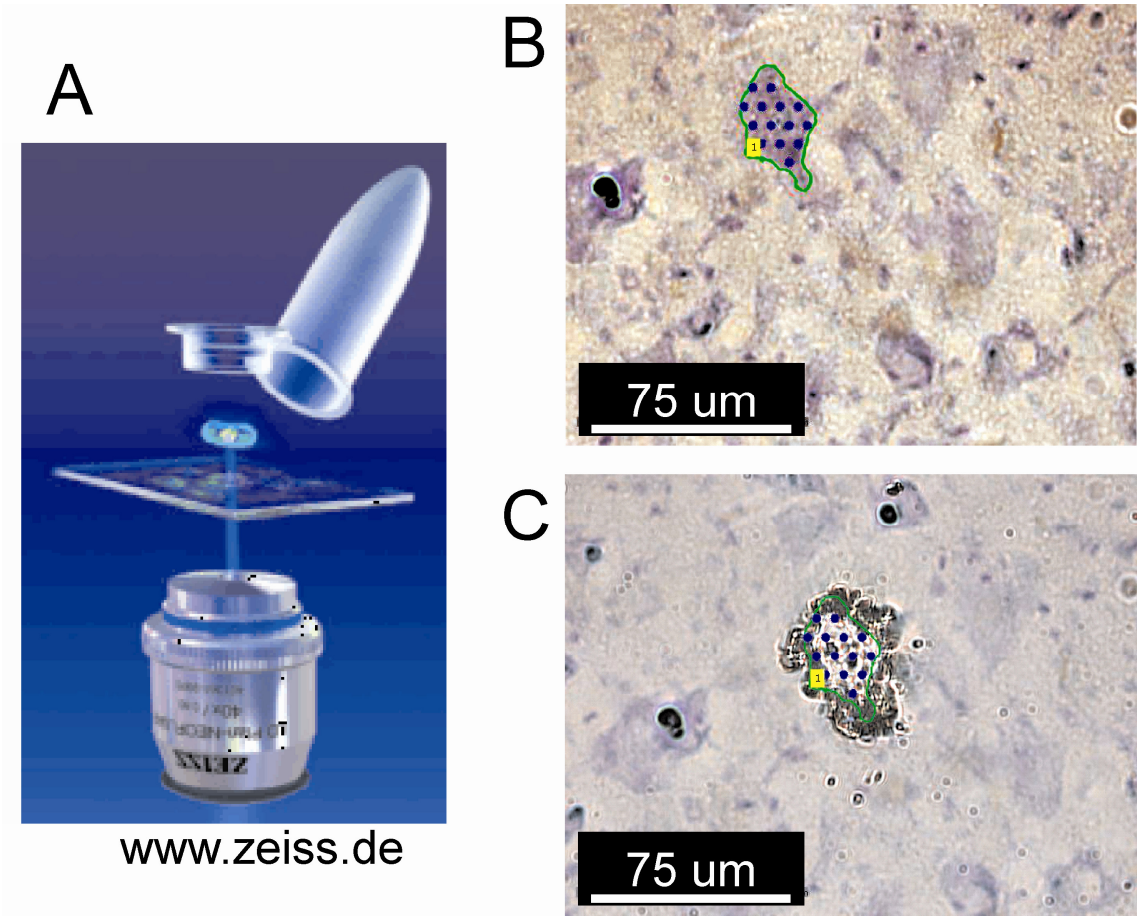

A) Laser microdissection technique allows isolating single cell or group of cells for further analysis (from www.zeiss.de). B) Motoneuronal somata stained with cresyl-violet. The green line is drawn around the perimeter of soma. Blue dots show sites where laser impulse is applied to catapult tissue inside area. C) The same wide-field image after motoneuron isolation shows empty cavity.

3. IMMUNOHISTOCHEMISTRY

For immunofluorescence staining, female rats (P1 and P8) were used. Lumbar regions of the spinal cord were fixed in Zinc Fixative (BD Pharmingen™) for 8-10 h and then kept in sucrose (30 % dissolved in Zinc fixative) for 10-12 h. Tissue was frozen in liquid nitrogen and sectioned at 16 µm with a cryomicrotome. Slices were washed in phosphate buffered saline (PBS) and processed with antibodies against CFTR (1:60, Lab Vision Products Thermo Fisher Scientific, Table 2), and KCC2 (1:600, Millipore/Upstate, Table 2) overnight at 4 °C. After washing in PBS immunofluorescence reactions were visualized using secondary antibodies labeled with AlexaFluor 488 or AlexaFluor 594 (1:500; Invitrogen) using wide-field and confocal microscopy. Co-staining experiments were performed with the anti-MAP2 antibody (Millipore, Table 2) against the microtubule-associated protein 2 to identify neuronal somata and dendrites. Cells stained with the secondary antibody only showed no immunostaining (Fig. 5). Quantitative analysis of immunofluorescence data was performed with MetaMorph software (Molecular Devices). The difference in signal intensity was calculated for somata between P1 and P8 by analyzing ≥ 15 somata in sections taken at these two ages for each experiment. The Metamorph software was used to automatically set the signal-to-noise ratio by selecting a certain fluorescence threshold level (throughout the whole image) that was kept constant for each experiment.

An antibody against NKCC1 (Millipore, Table 2) was also used. However, since the specificity of the antibody against NKCC1 is doubtful (Blaesse et al., 2009; Prof. Kaila, personal communication), it was important to test the antibody first. Dr Peter Blaesse and

Prof. Kai Kaila from University of Helsinki kindly provided NKCC1 knockout tissue. Figure 6 demonstrates that NKCC1 antibody was not specific, and it was not used for immunohistochemical experiments.

Table 2. Antibodies used for immunohistochemistry.

Antibody	Type	Epitope	Source	Dilution	References
CFTR	Monoclonal (L12B4))	aa 386-412	Thermo Fisher Scientific	1:60	Kartner et al. (1992)
KCC2	Polyclonal	N/A	Upstate (Millipore)	1:600	Williams et al. (1999)
NKCC1	Polyclonal	N/A	Chemicon (Millipore)	1:60	Kaplan et al. (1996)
Map 2	Polyclonal	N/A	Millipore	1:500	Díez-Guerra and Avila (1993)

Figure 5. Control staining with the secondary antibody.

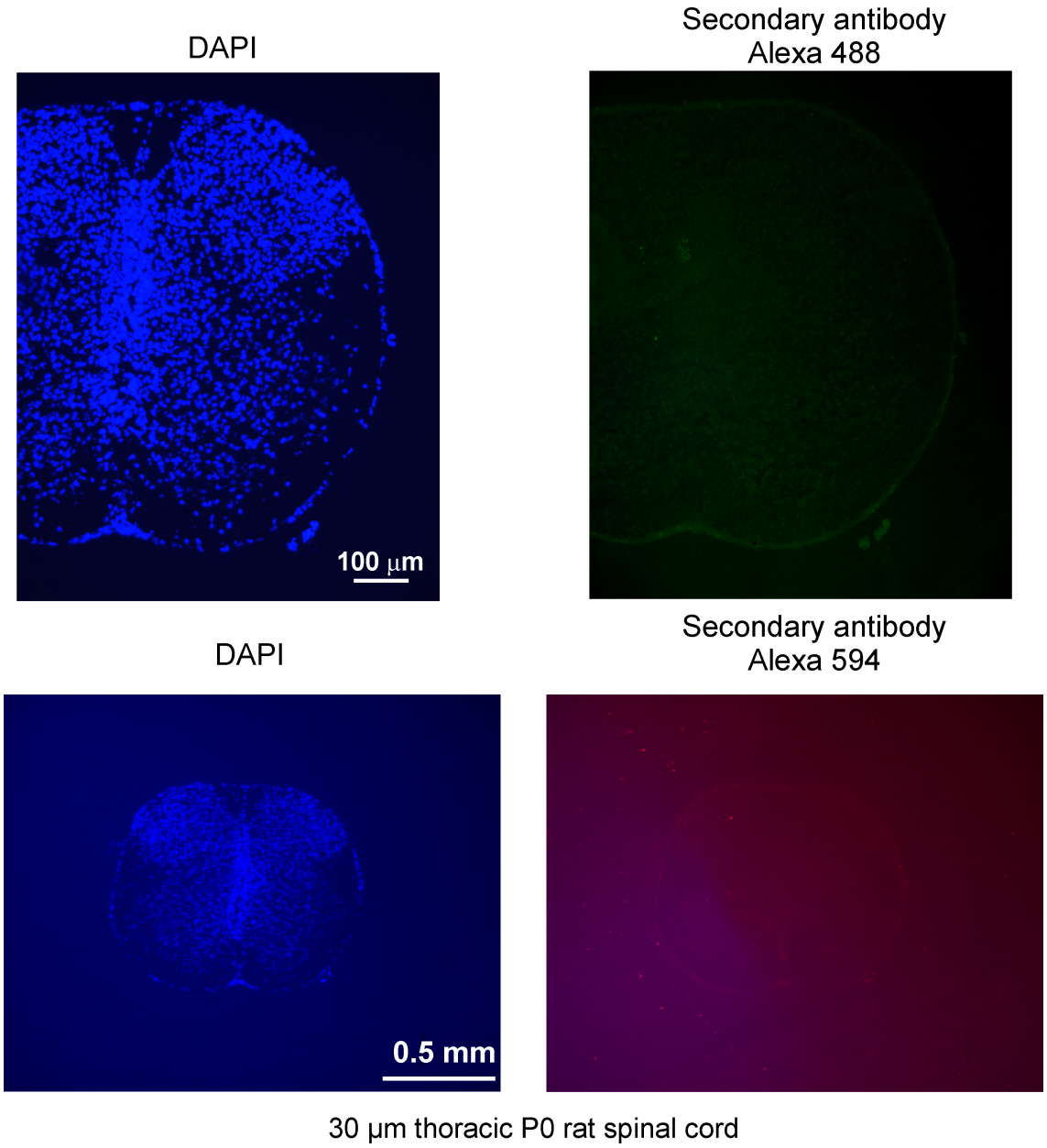

Image showing staining with the secondary antibody only (on the right). 4',6-diamidino-2-phenylindole (DAPI; binds strongly to DNA) staining is shown on the left. Images were kindly provided by Dr. Miranda Mladinic.

Figure 6. Comparison of anti-NKCC1 antibody staining in coronal sections of mouse wild-type and NKCC1 knockout brain at P0.

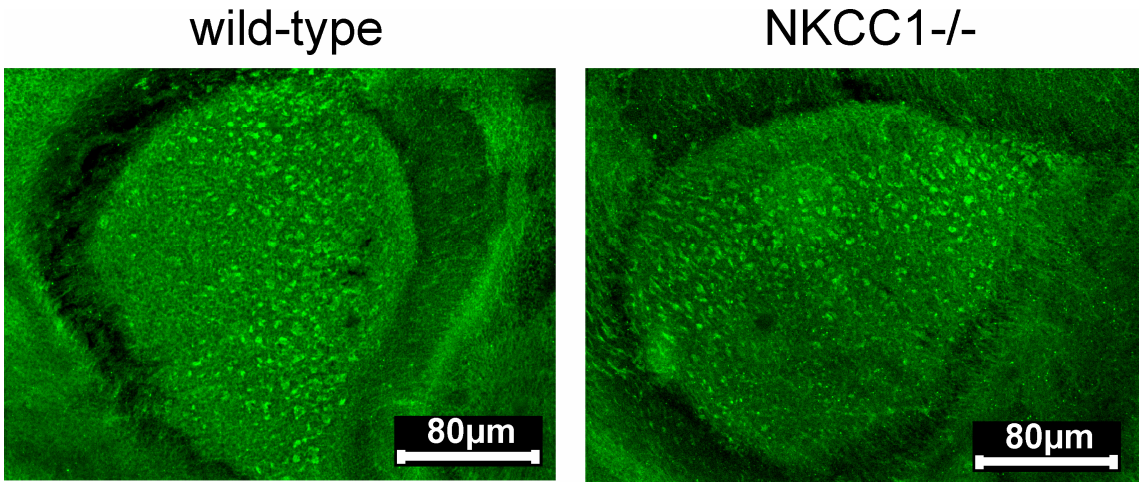

Coronal sections of the forebrain of the rat show substantial numbers of immunopositive cells in either wild-type or knockout animals. This observation confirms the lack of NKCC1 specificity of the commercially-available antibodies (see also Blaesse et al., 2009).

4. ELECTROPHYSIOLOGY

4.1 Recording chamber for electrophysiological experiments and viability of the spinal cord

After dissection, the hemisected spinal cord was pinned (medial side upwards) to the sylgard bottom of a recording chamber made of plexiglass (internal volume ~ 3 ml) and was continuously perfused with ACSF. Perfusion was fed by a peristaltic pump that delivered oxygenated ACSF to the recording chamber, via small tubing, parallel to the rostrocaudal axis of the spinal cord and ACSF outflow was drained via small channel.

Constant flow rate was ensured by a flow spacer placed between the pump and the chamber to damp fast oscillations in the fluid level. Flow was maintained between 5 and 7 ml/min. All chemicals were applied via the perfusion system. The time necessary to completely exchange the solution in the bath was estimated using ACSF stained with phenol red and found to be less then 3 min.

Miniature suction bipolar electrodes were used in order to deliver single or repetitive electrical stimuli to either DR or VR. Such electrodes were made from thin (1.5 mm diameter) glass capillaries and contained a silver wire inside and another one wound around. Electrode tip diameter was chosen to closely fit the root to be stimulated. Roots were sucked into the electrode by applying gentle negative pressure with a syringe connected to the apical end of the pipette. Square electrical pulses (0.1 – 0.2 ms duration, 0.5 – 10 V amplitude) were applied via a Grass S88 (Grass Medical Instruments) stimulator to either DRs to activate afferent fibers, or to VRs in order to antidromic stimulate motoneurons.

After dissection, the viability of the spinal cord was ascertained before any further testing. In healthy preparations, single pulse stimulation delivered to one DR elicited a reflex response from the ipsilateral VR at the same segmental level. If this response was absent, the preparation was discarded.

4.2 Intracellular recording

Intracellular recording from lumbar motoneurons at P1 and P8 was performed with sharp glass electrodes filled with 2M K-acetate and connected via 0.1x headstage (Axon instruments) to an amplifier (Axoclamp 2A, Axon instruments). Electrode resistance varied between 110 and 180 MΩ.

As the sharp electrode was lowered into the ventral spinal cord, the following stimulation protocol (delivered at frequency of 2 Hz) allowed motoneurons to be identified: a negative current step (10 ms, 0.5 nA) for monitoring electrode resistance, followed, with a 50 ms lag, by a pulse stimulus (0.1 ms duration) applied to the ipsilateral homologous VR (antidromic stimulation).

When the electrode was in the proximity of the motor nucleus, antidromic stimulation evoked a short latency (~ 2 ms) biphasic field potential due to a synchronous motoneuron firing (Fulton and Walton, 1986), while the increase in the electrode resistance was used as a sign that the tip of the electrode was in contact with the membrane of the motoneuron. At this stage, the "clear" command of the amplifier was applied in order to facilitate penetration into the membrane.

Current-clamp experiments were performed in bridge mode. In such conditions, the variable current step is known to cause a corresponding voltage drop across the micropipette that adds up to the cell potential in a time-independent fashion. A special compensation circuitry can be used to eliminate the micropipette voltage from the recording. Thus, the bridge mode compensation generates a signal that is proportional to the product of the micropipette current and the micropipette resistance: this signal is then

subtracted from the buffer amplifier output. By using manually this facility on the Axoclamp amplifier it was possible to eliminate the instantaneous voltage component. The accuracy of the bridge compensation was routinely checked during the experiment. After motoneuron impalement, VR stimulation elicited a short latency (<2 ms) all-or-none, overshooting antidromic action potential (Fulton and Walton, 1986). Only cells in which this kind of response could be consistently elicited were considered for analysis.

Electrode capacitance was compensated by injecting a current into the cell in Discontinuous Current Clamp mode (DCC; 1.5-2.0 Hz sample rate). In DCC mode the capacitance neutralization control plays a similar role to the Bridge Balance control in continuous current clamping. Tuning the "Capacitance Compensation" facility determines what fraction of time will be used for passing current and what for measuring voltage at a preset frequency of switching between these two modes. With the aid of an oscilloscope, which continuously monitored the amplifier head-stage output, it was possible to see the shape of the waveforms that was optimized (by manually tuning sampling frequency and capacitance compensation) to allow full decay of the transients (induced after the current pulses) to baseline before the next cycle at the maximum frequency.

Motoneuron input resistance at rest was continuously monitored by injecting a negative current pulse (20-50 ms) and then calculated as the ratio between the steady state hyperpolarization amplitude induced by injection of the pulse and the amplitude of the current injected. Bridge balance was routinely monitored and compensated whenever necessary. To monitor the voltage-dependence of single cell responses, current-voltage (I-V) curves were performed. In this case, successive hyperpolarizing (0.01 to 0.1 nA,

with 0.01 nA intervals) and depolarizing (0.01 to 0.1 nA, with 0.01 nA intervals) current steps were delivered at 0.2-0.5 Hz.

The function of CFTR was investigated with the sulphonylurea glibenclamide (Tocris Bioscience), a well-known CFTR blocker at the concentration of 50 µM (Schultz et al., 1999). Electrical properties of motoneurons like input resistance, spike amplitude and membrane potential were analyzed before and after drug application via the bathing solution. Input resistance was calculated from the slope of the voltage/current plots. Fast synaptic transmission was blocked by 4-hydroxyquinoline-2-carboxylic acid (kynurenic acid, 3 mM), strychnine hydrochloride (1 µM), and bicuculline methiodide (20 µM) (all from Sigma-Aldrich). Analysis was performed with Clampfit 9.2 software (Molecular Devices).

4.3 Whole-cell patch clamp recording

The whole cell patch-clamp technique was applied to sagitally hemisected spinal cords at P1 and P8 (Fig. 7 A). Patch pipettes had resistance of 4-7 MΩ and contained in mM: 125 K-gluconate, 5 KCl, 5 NaCl, 2 $MgCl_2$, 10 HEPES, 10 EGTA, 2 ATP-Mg salt, pH 7.2. Constant positive air pressure was applied to the pipette interior while lumbar motoneurons were approached blindly through the medial (cut) surface of the spinal cord in current clamp mode as described in the previous section, although the Axopatch 1D (Axon Instruments) amplifier was used for patch clamp experiments.

Similar to the experiments with the sharp electrode, biphasic field potential together with the increase in the electrode resistance were used as a sign that the tip of the electrode

was in contact with the membrane of the motoneuron. Gentle suction, applied to the pipette interior, led to the formation of an electrical seal with the resistance in the order of 2-10 GΩ (giga-seal). After the giga-seal formation the amplifier was switched to voltage-clamp mode and the holding potential was set to -70 mV. After that step, additional suction applied to the pipette interior led to membrane rupture, and enabled low resistance access to the cell interior.

Motoneurons were normally held at a potential value corresponding to 0 net current flow (resting potential) which was in the range -75 to -85 mV and series resistance was routinely monitored without any compensation. All-or-none, overshooting antidromic action potentials were elicited at the beginning and at the end of each experiment switching the recording to current clamp mode for a short period of time. Only cells in which this kind of response could be consistently elicited and whose series resistance was not altered for more than 30% during an experiment, were considered for analysis.

The junction potential from pipette to the external solution (-13 mV) was corrected offline based on the composition of the internal and external solutions used for recording. Using these transmembrane concentrations of Cl^- and disregarding the operation of anion transporters, the Nernst equation provided a theoretical $E_{GABA/Gly}$ of -57 mV. During electrophysiological recording, the actual estimate of the $E_{GABA/Gly}$ value was obtained as previously described (Gonzalez-Islas et al., 2009). Namely, spontaneous events were recorded in the presence of 3 mM kynurenic acid in voltage clamp mode. Voltage steps were given for 15-60 sec in 5 mV increments usually from -110 to -40 mV. The average amplitude of spontaneous postsynaptic currents (sPSCs) at each step was plotted against voltage. The potential value read at zero amplitude of sPSCs was taken as the reversal

potential. Potential values near the actual reversal potential were avoided to remove uncertainty about calculating the size of small amplitude sPSCs close to the background noise (Fig. 7 B, C). The influence of CFTR or NKCC1 on Cl^- homeostasis was estimated by comparing reversal potentials before and after applying of 50 µM glibenclamide or 10 µM bumetanide (Sigma-Aldrich), respectively.

Figure 7. Estimation of $E_{GABA/Gly}$ in whole-cell patch clamp experiments.

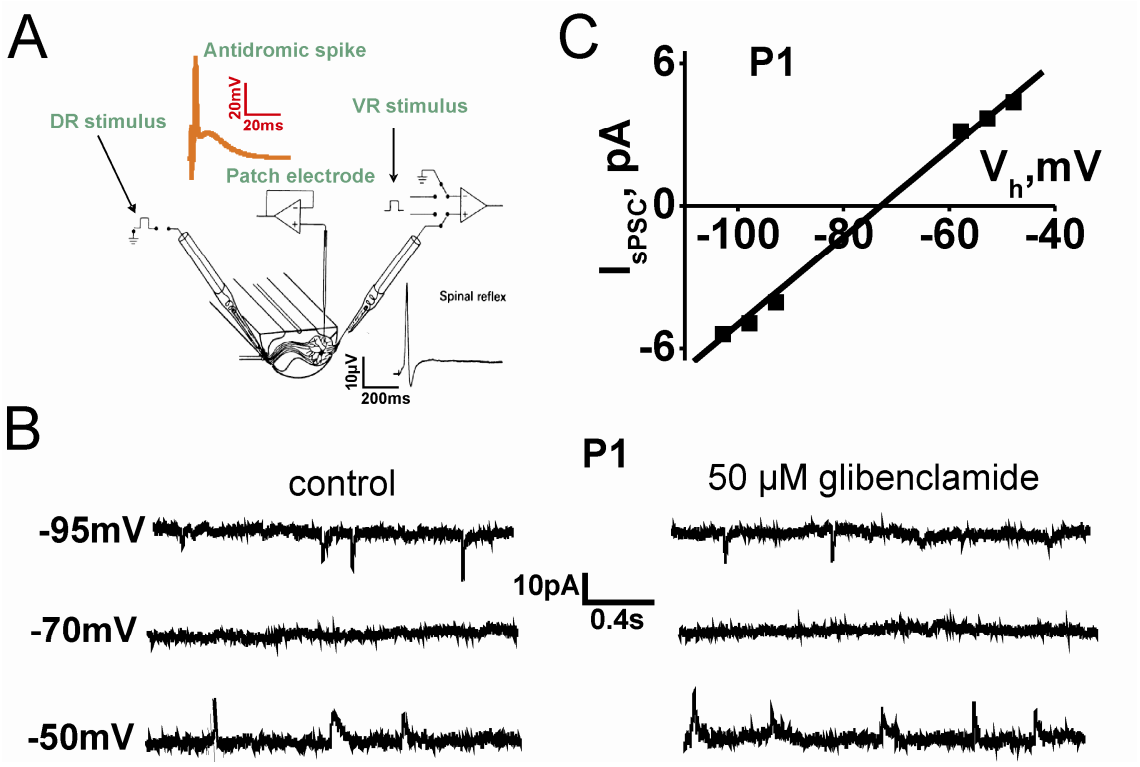

A) Experimental configuration for patch clamping of motoneurons. DR was stimulated to elicit a reflex response from the ipsilateral VR at the same segmental level, therefore to check viability of hemisected spinal cord. Lumbar motoneurons were approached blindly with the patch pipette through the medial (cut) surface of the spinal cord and were identified by their antidromic response to VR stimulation in current clamp mode. B) An example of continuous recordings from motoneuron at P1. sPSCs were recorded at different holding potentials before and after glibenclamide application. C) An example of $E_{GABA/Gly}$ estimation for P1 motoneuron.

5. MODELING

5.1. A 3D model of the motoneuron

A 3D model of the neonatal rat lumbar motoneuron was reconstructed in accordance with the recent study by Ostroumov (2007). Random 3D morphologies of the rat spinal motoneurons, which correspond to a predetermined set of morphological global parameters describing these neurons during the first postnatal week (Table 3), were generated in MATLAB version 7.1 Release 14 (The MathWorks Inc.). Subsequently, voltage-dependent ionic currents necessary for spike generation and passive properties of motoneuronal membranes (Table 4, 5) were introduced into the model using the NEURON simulation environment (version 5.7; Hines and Carnevale, 1997). Just three voltage-dependent conductances were introduced into the model, namely, Na^+, transient K^+ (K_A) and delayed rectifier (K_{dr}). These conductances distributed through the cell surface are sufficient to generate action potentials (Lüscher and Larkum, 1998; Safronov et al., 2000). Passive properties were specific membrane resistance, R_m, axial resistance, R_a, and specific membrane capacitance, C_m. They were defined following Thurbon et al., (1998) and were equal for all cell compartments. Since during the first postnatal week there is an increase in motoneuronal size (Fulton and Walton, 1986), developmental changes in motoneuron morphology were simulated by changing the mean diameters of the soma.

5.2. Simulating the effect of CFTR on the input resistance

The developmental effect of the CFTR inhibition on input resistance of motoneurons was mimicked by changing the specific membrane resistance (R_m) of different compartments as indicated by the developmental regulation of CFTR expression observed in the present study. To this end, R_m was defined as the resistance of one square centimeter of membrane. If dealing with a neuron that could be modeled as a single soma compartment, then the input resistance would simply be given by the membrane resistance, $R_{in} = R_m/\text{area}$. When there are other compartments, then the axial resistances (R_a) and membrane resistances of these compartments also add to the resistive load, and the expression becomes more complicated. For a simple model with a few compartments, circuit theory can be used to calculate R_{in} in terms of R_m, R_a, and the compartment dimensions. In the case of an infinite cylinder, the equation is (Segev, 1998)

$R_{in}=(1/\pi)\cdot d^{-3/2}\cdot(R_m\cdot R_a)^{1/2}$, where d is the diameter of an infinite cylinder.

Thus, changes in R_m values induced by experimental conditions are not directly transferred into variations of R_{in} of analogous magnitude.

5.3. Estimating CFTR impact on motoneuronal excitability

In order to replicate closely passive and active properties of motoneurons the model implies a resting membrane potential value of -70 mV. The driving force for Cl^- (membrane potential minus the reversal potential) was then set as -10 mV as detected experimentally at P1. The role of changes in $E_{GABA/Gly}$ produced by glibenclamide was

investigated by simulating action potential (AP) initiation (trigger by a 5 ms depolarizing pulse) occurring together with the inhibitory postsynaptic potential (IPSP) whose parameters were similar to those recorded for the recurrent IPSP by Marchetti et al. (2002) and used by Jean-Xavier et al. (2007) (4-8 mV amplitude and the time constant between 20 and 70 ms). Electrotonic depolarizing potentials induced by subthreshold current pulses were used to simulate excitatory postsynaptic potentials (EPSPs). The kinetics of the recurrent IPSP were described by an α-function conductance given by $I=g\cdot(V-E)$, where I is the synaptic current (nA), g is the synaptic conductance (μS) calculated as $g=gmax\cdot t/\tau\cdot(\exp(1-t/\tau)$ with gmax equal to the maximum conductance for the postsynaptic inhibitory channels, t is time (ms) and τ is the time constant of synaptic potential decay, V is the motoneuron membrane potential (mV), and E is the equilibrium potential (mV) for the ion(s) permeating through the open channels. The value of E was adjusted for the recurrent IPSPs in accordance with physiological measurements of $E_{GABA/Gly}$ before and after glibenclamide application at different developmental ages.

Table 3. Motoneuronal simulated morphological characteristics

SOMA	
Minor diameter, µm	19.6±5.5
Major diameter, µm	31.51±8.28
AXON	
Axon hillock diameter, µm	3
Axon hillock length, µm	8
Initial segment diameter, µm	0.8
Initial segment length, µm	10
Axon proper diameter, µm	0.8
Axon proper length, µm	500
PROXIMAL DENDRITES	
Number, µm	6.3±1.8
Diameter, µm	3.16±1.42
Maximal length, µm	25
DISTAL DENDRITES	
Branching maximal order, µm	5.1±1.3
Rall's ratio, µm	0.89±0.13
First group maximal length, µm	40
Second group maximal length, µm	70
Third group maximal length, µm	85

Table 4. Distribution of voltage-gated conductances through the motoneuron surface

	INa, S/cm^2	IK_A, S/cm^2	IK_{dr}, S/cm^2
Soma	0.113	0.218	0.029
Proximal dendrites	0.003	0	0.001
Distal dendrites	0.003	0	0.001
Axon hillock	0.7	0	0.11
Initial segment	0.7	0	0.11
Soma proper	0.012	0	0.04

Table 5. Passive properties of motoneuronal membrane

Specific membrane resistance (R_m), kΩ·cm^2	Specific membrane capacitance (C_m), μF/cm^2	Axial resistance (R_a), Ω·cm
5.3	2.4	87

6. STATISTICAL ANALYSIS

Statistical analysis was performed using nonparametric tests, namely the Mann-Whitney Rank Sum test and the Kruskal-Wallis followed by Tukey post-hoc test when comparison was made for more than two groups. Results are presented as mean±standard error (SE). Data correlation was expressed using the Spearman rank correlation.

RESULTS

1. CFTR, NKCC1 AND KCC2 GENE EXPRESSION IN THE RAT SPINAL CORD DURING POSTNATAL DEVELOPMENT

Real-time RT PCR experiments were performed to look at dynamical change in gene expression at different ages and sex of the animal. For neuronal KCC2, the neuron-specific β-tubulin III was used as a housekeeping gene. In all other cases GAPDH was used as reference.

1.1. Sex-dependent differences in gene expression and neuronal content of the spinal cord at P1 and P8

At first, CFTR, NKCC1 and KCC2 mRNA levels were compared between male and female rats at P1 and P8, since former studies on brain tissue reported sex-difference in NKCC1 and KCC2 gene expression (Galanopoulou et al., 2003; Nuñez and McCarthy, 2007; Perrot-Sinal et al., 2007). In the neonatal lumbar spinal cord, KCC2 mRNA was 1.7±0.4 times higher in females compared to males at P1 ($p<0.05$, number of spinal cords, n=5, Fig. 8 A). At P8 the difference between male and female tissue was even larger for KCC2 (2.2±0.7, $p<0.05$, n=5, Fig. 8 A). Conversely, the β-tubulin III gene was less expressed in females than in males (0.7±0.1 at P1, 0.7±0.2 at P8, $p<0.05$, n=5, Fig. 8 B). No significant difference between males and females was found for CFTR and NKCC1 gene expression at both P1 and P8 (Fig. 8 C, D).

Figure 8. Cl^- transporter genes in males and females.

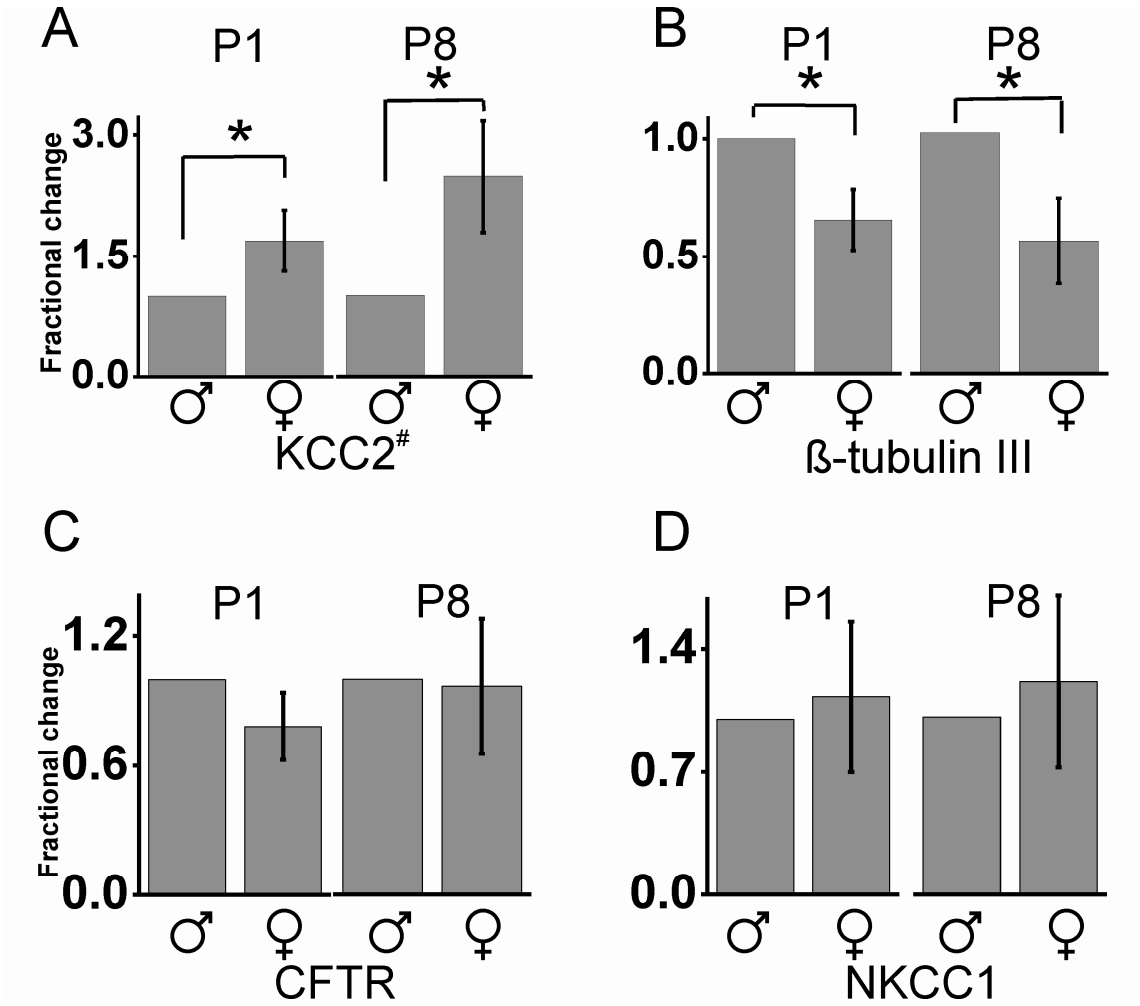

A, B) KCC2 and β-tubulin III gene expression between males (♂) and females (♀) at P1 and P8. At both ages, the synthesis of KCC2 mRNA is higher in females compared to males, whereas β-tubulin III mRNA is lower (*$p<0.05$, n=5). C, D) No statistically significant difference between males and females at both ages for CFTR and NKCC1 was found (n=5).

1.2. Developmental changes in gene expression

I, therefore, investigated gene transcription for KCC2, CFTR and NKCC1 at P1, P4, P6 and P8 separately for male (top row) and female (bottom row) spinal cord tissues (Fig. 9). The KCC2 signal increased from P1 to P8 reaching the maximum at P6 in males (2.2±0.2, $p<0.03$, n=6) and at P8 in females (3.0±0.4, $p<0.03$, n=5). In accordance with the phenomenon of developmental loss of neurons (Bennett et al., 1983), age-dependent decrease in β-tubulin III gene expression was observed (Fig. 9, right). Within this age span, the lowest signal was at P6 in males (0.44±0.05, $p<0.03$, n=6) and at P8 in females (0.32±0.03, $p<0.03$, n=5). Gene expression of NKCC1 increased twice from P1 to P8 in the neonatal lumbar spinal cord for both sexes ($p<0.03$, n=6 for males, n=5 for females, Fig. 9). As shown in Figure 9, the signal for CFTR mRNA also rose with development in males (1.7±0.1 at P8, $p<0.03$, n=6) and in females (2.1±0.4 at P6, $p<0.03$, n=5).

Figure 9. Developmental changes in gene expression in males (♂) and females (♀).

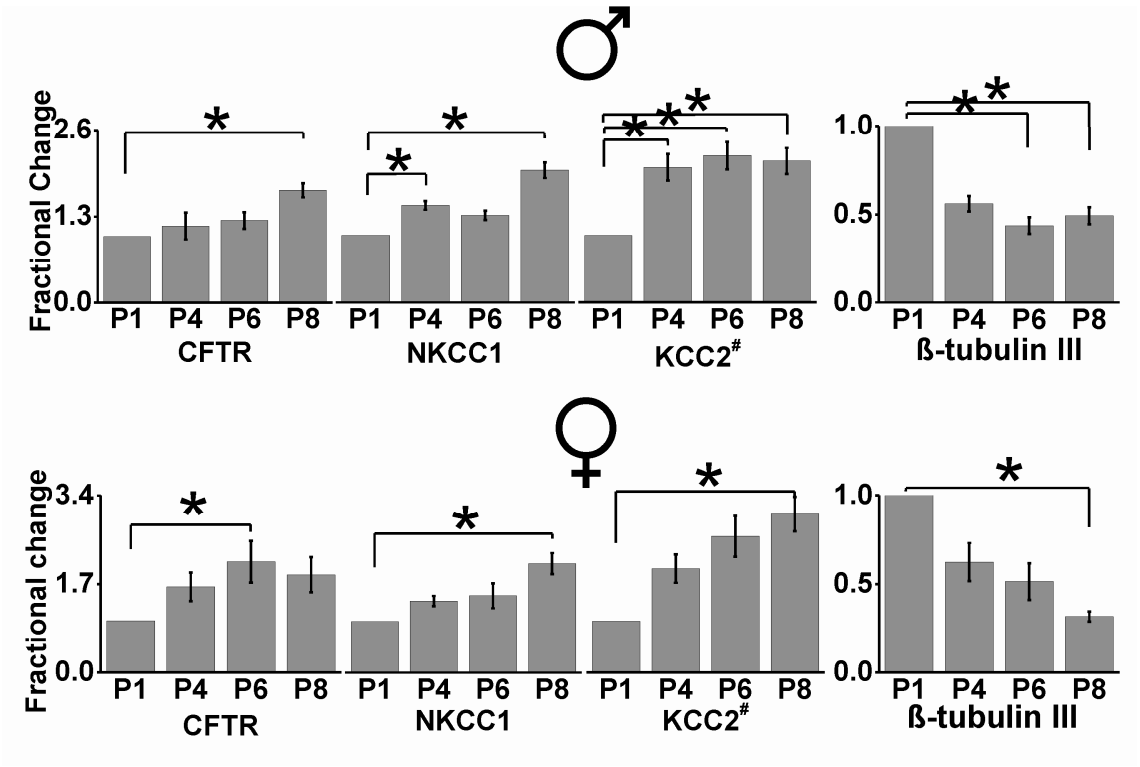

Signals for CFTR, NKCC1 and KCC2 increase between P1 and P8 in both genders (*p<0.03, n=6 for males and n=5 for females).

1.3. Age dependent correlation between CFTR and NKCC1

Because of the former hypothesis of a functional link between CFTR and NKCC1 (Ostroumov et al., 2007), it was important to investigate any correlation between CFTR and NKCC1. The relative increase of these genes at P4, P6 and P8 was analyzed in 5 experiments. The correlation coefficient r was obtained using Spearman rank correlation and had the value of 0.741 for male and 0.781 for female tissues (n=5, p<0.002; Fig. 10). No similar correlation was found between CFTR and KCC2, or NKCC1 and KCC2 for either sex. The correlation coefficients for CFTR vs KCC2 had the value of 0.079 for

males and 0.179 for females (n=5, p>0.5). And for NKCC1 vs KCC2 the correlation coefficients were equal to 0.279 for males and 0.356 for females (n=5, p>0.2).

Figure 10. Developmental correlation between CFTR and NKCC1 PCR signal for males (♂) and females (♀).

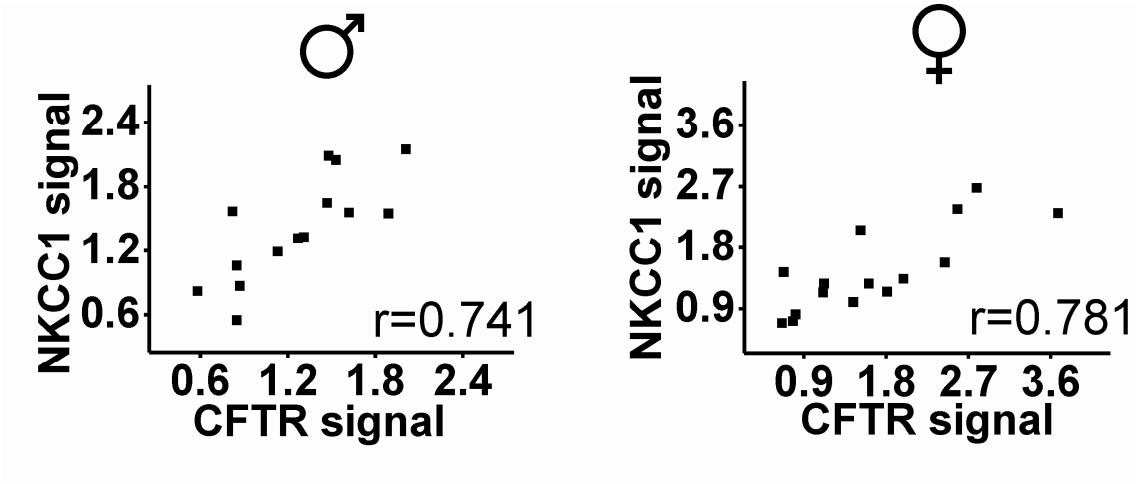

1.4. Laser capture microdissection

Being interested in developmental changes in CFTR, NKCC1 and KCC2 gene expression in motoneurons, it was possible to isolate this type of cell using Laser Microdissection and Pressure Catapulting technology and perform real time RT PCR. To obtain a strong PCR signal it was necessary to collect at least 200 cells. Considerable S100B (a marker of astrocytes, Kuzhandaivel et al., 2010; Wang and Bordey, 2008) signal showed that there was a substantial contamination of motoneuron samples with astrocytes. This observation indicated that such motoneuron samples could not be further used to study the neuronal changes in CFTR or NKCC1 because these proteins are not neuron-specific.

2. IMMUNOHISTOCHEMISTRY OF CFTR AND KCC2

Antibodies against CFTR and KCC2 were used to determine the presence of these proteins in the female neonatal lumbar spinal cord at P1 and P8. Unfortunately, there was no commercially available specific antibody against NKCC1 (Blaesse et al., 2009).

2.1. CFTR expression in motoneurons

Fig. 11 A shows that large cells in the ventral horn of the spinal cord were stained by the CFTR antibody. These cells were considered to be motoneurons because of their large somata (>20 µm diameter) and laminar location (Molander et al., 1984). Finally, co-staining experiments with the neuronal marker Map2 were performed. Cells which were positive to CFTR antibody were also identified by Map2 (Fig. 11 B).

Expression of CFTR protein was studied in P1 and P8 lumbar segments. CFTR expression apparently increased in cell processes and fibers from P1 to P8 (see example in Fig. 11 C). However, it was difficult to follow up its distribution within the dense neuronal mesh. Thus, the difference in signal intensity for somata between P1 and P8 was calculated by analyzing $\geq$ 15 somata of these two ages for each experiment using MetaMorph software (figure 12 A). A CFTR positive soma was considered to be a motoneuron and marked out only if it was localized in the ventral part of the spinal cord, had a diameter of at least 20 µm and had an identifiable nucleus. The significant increase (30% on the average; $p<0.001$) in somatic CFTR signal intensity from P1 to P8 was systematically found, while the signal-to-noise ratio was the same (Fig. 12 B).

Figure 11. CFTR immunohistochemistry in the lumbar spinal cord.

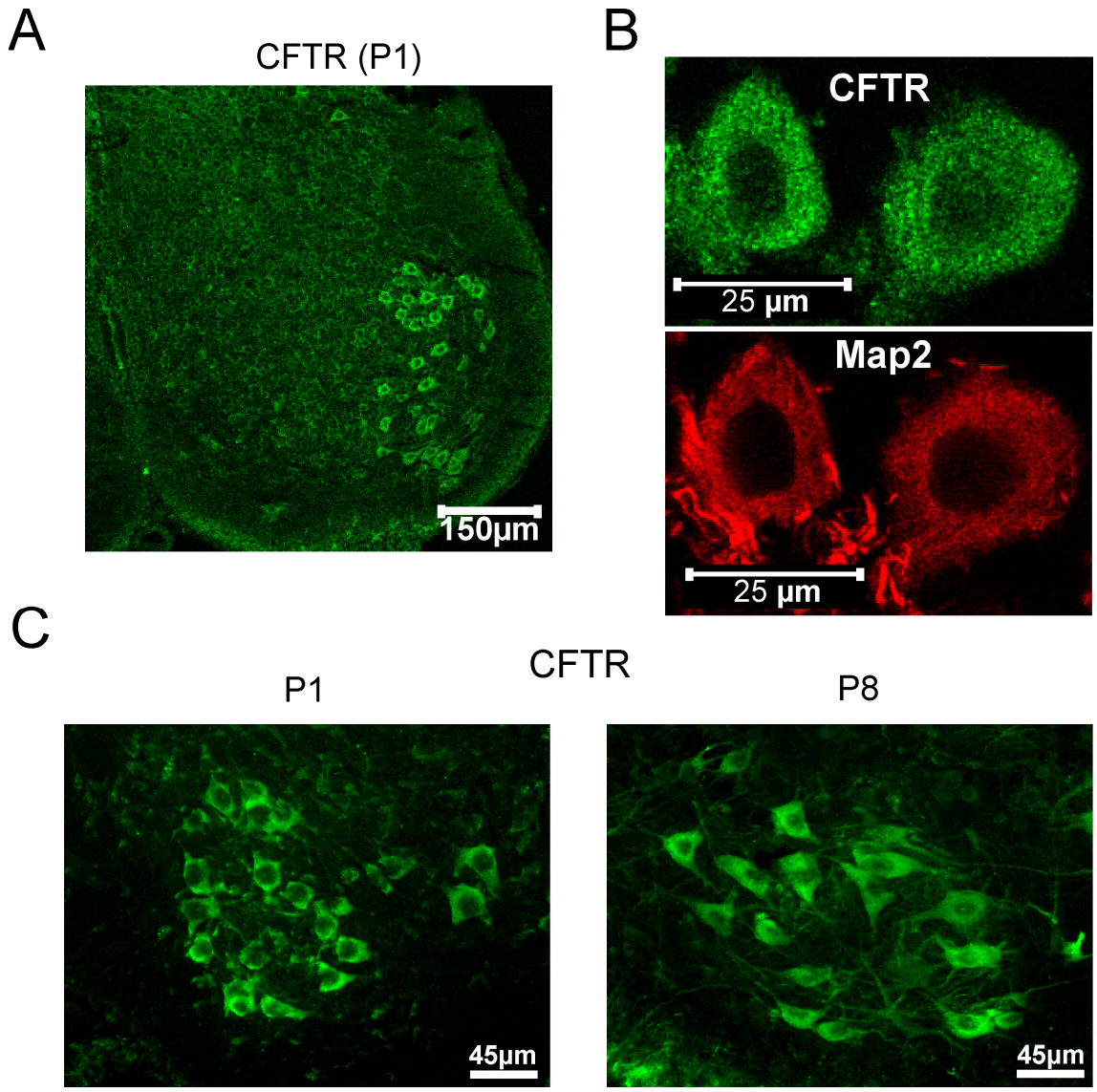

A) Confocal image showing immunohistochemical staining with anti-CFTR antibody in the ventral part of lumbar L3-L5 segment of P1 animal. B) Confocal image of motoneurons positive for CFTR and the neuronal marker Map2. C) Images showing staining with anti-CFTR antibody in P1 and P8 spinal cords. Images were taken using wide-field microscopy.

Figure 12. CFTR signal intensity measuring in motoneuronal somata at P1 and P8.

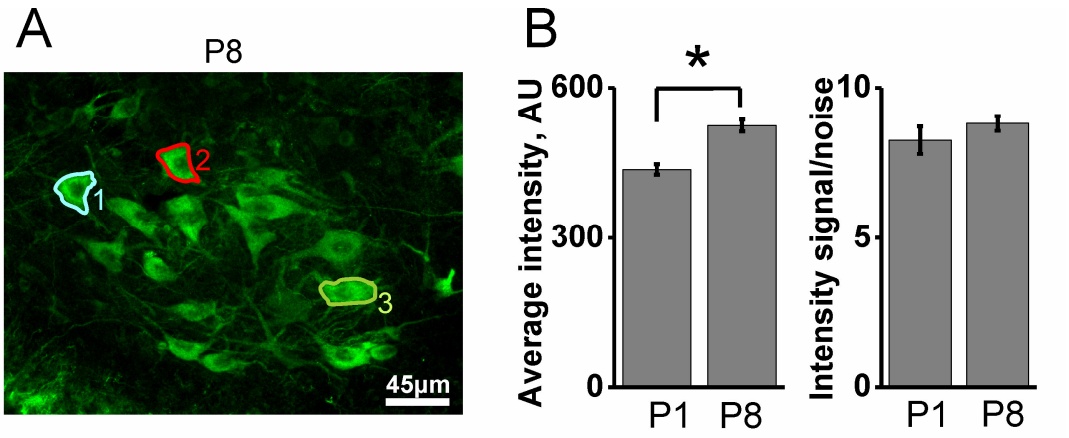

A) Signal intensity was estimated inside the CFTR positive somata, which localized in the ventral part of the spinal cord; had a diameter of at least 20 µm and had an identifiable nucleus. An example from P8 shows marked out regions of interest (1, 2 and 3) where intensity was calculated using MetaMorph Software. B) Stronger CFTR signal intensity at P8 vs P1, while signal/noise ratio for somata between P1 and P8 is similar (* $p<0.001$, $n=16$; experiments run in triplicate).

2.2. KCC2 expression in the rat lumbar spinal cord

To analyze age-dependent changes in the amount and distribution of KCC2 in motoneurons, KCC2 immunoreactivity at P1 and P8 was analyzed in the ventral horn of lumbar spinal cords. Already at P1 a very strong signal widely distributed through the ventral horn and mainly expressed in cell processes surrounding cell bodies was indicated (Fig. 13 A, left; see also Jean-Xavier et al., 2006). At P8, the labeling pattern was similar in that the somata and processes were again outlined (Fig. 13 A, right). A method to estimate somatic signal intensity, similar to the one used for CFTR, showed that there was no difference in somatic KCC2 signal in the ventral horn between P1 and P8.

However, the staining became more distinct at P8 (Fig. 13 B for higher magnification). The reduction in diffuse labeling was reported by Blaesse et al. (2006) for the developing rat lateral superior olive, and was explained as the consequence of pruning the dendrites.

Figure 13. KCC2 immunohistochemistry in the lumbar spinal cord.

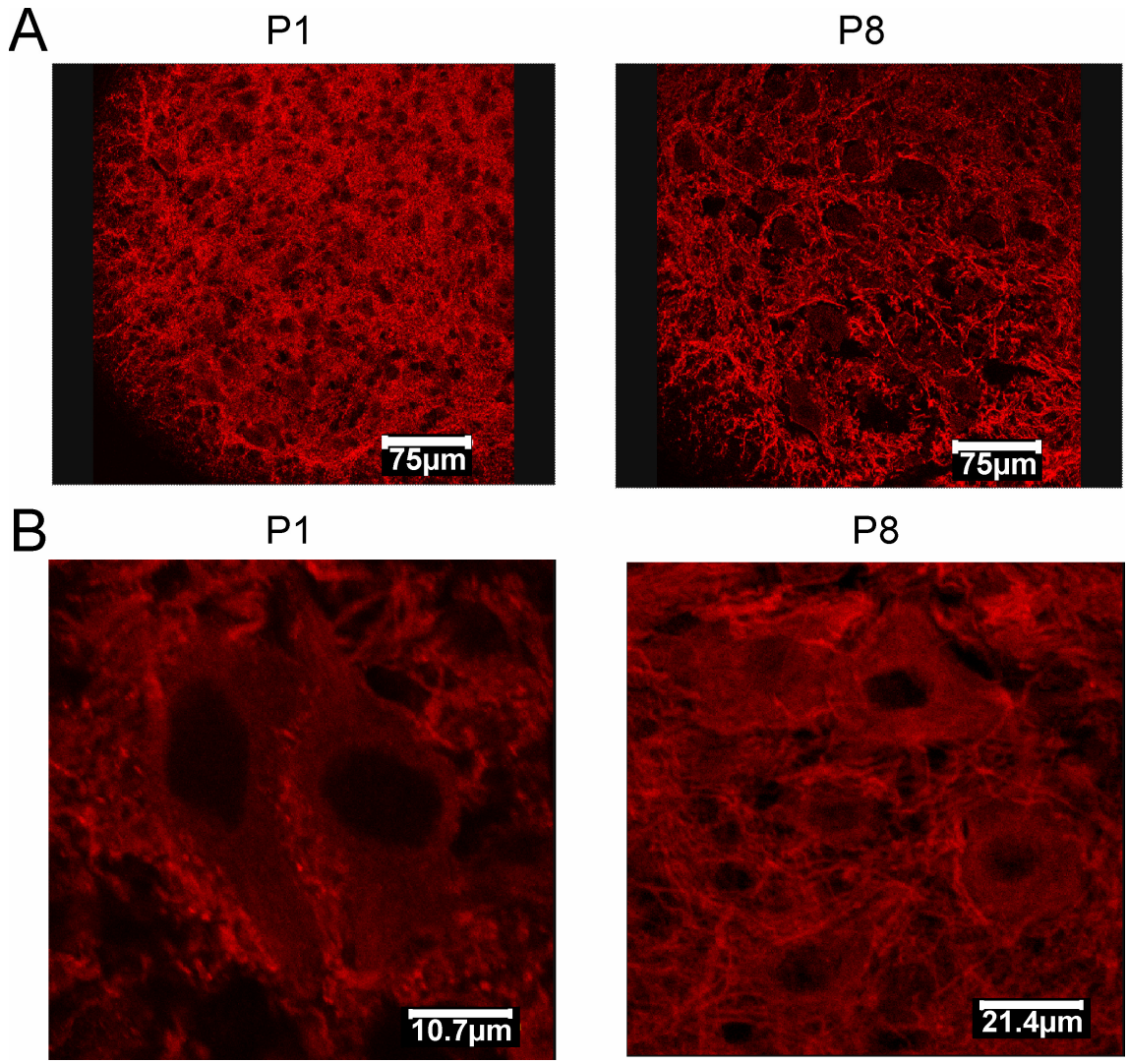

A) Confocal images showing staining with anti-KCC2 antibody in P1 and P8 spinal cords. B) Higher magnification confocal images showing staining with anti-KCC2 antibody at P1 and P8.

3. FUNCTIONAL CONSEQUENCES OF CFTR INHIBITION

Ostroumov et al. (2007) have shown the effect of the CFTR sulphonylurea blocker glibenclamide (50 μM) on the electrophysiological properties of rat lumbar motoneurons at P4-P8. In the present study, the action of CFTR at earlier postnatal days (P0-P2) was clarified first, and then its impact on Cl^- homeostasis during the first postnatal week was explored.

3.1. Electrophysiology of lumbar motoneurons studied with sharp electrode technique

To explore the effect of glibenclamide on the electrophysiological properties of rat lumbar motoneurons, these cells were recorded from the sagittally hemisected spinal cord at P1 and P8 in the presence of fast synaptic transmission inhibitors (3 mM kynurenic acid, 20 μM bicuculline, and 1 μM strychnine) to prevent network dependent effects (Ostroumov et al., 2007). For these initial experiments, sharp electrodes (containing 2M K acetate) were employed since it was important to minimize any perturbation to the intracellular Cl^- concentration. In control solution (containing the synaptic blockers), membrane potential was similar for both ages (pooled average = -71.9±2.8 mV, Table 6). Motoneurons had input cell resistance of 39.4±5.6 MΩ at P1 and 17.1±2.0 MΩ at P8 ($p<0.005$; n=5 and 4, respectively). The amplitude of the antidromic action potential was significantly higher at P1 than at P8 (83.4±1.5 mV and 77.5±1.4 mV respectively, $p<0.03$, n=7; Table 6). At P8 glibenclamide increased input resistance (31±10%, $p<0.05$, n=4; Fig. 14 A, B) and produced slow membrane potential hyperpolarization

(2.4±0.7mV, $p<0.01$, n=4; Fig. 14 C), in analogy with the effects of similar magnitude as reported earlier (Ostroumov et al., 2007). Basic electrophysiological properties of P1 motoneurons were also affected by glibenclamide that increased input resistance (25.8±6.9%, $p<0.01$, n=5; Fig. 14 B) almost as much as at P8, and hyperpolarized membrane potential (1-2 mV).

Table 6. Electrophysiological properties of lumbar motoneurons at P1 and P8 obtained with sharp electrode recordings.

	Membrane Potential, mV (±SE)	Input Resistance, MΩ (±SE)	Spike Amplitude, mV (±SE)
P1	-72.7±2.3 (n=5)	39.4±5.6 (n=5)	83.4±1.5 (n=7)
P8	-71.1±2.8 (n=4)	17.1±2.0 (n=4)	77.5±1.4 (n=7)

Figure 14. Effect of 50 µM glibenclamide on electrical properties of L3-L5 motoneurons at P1 and P8.

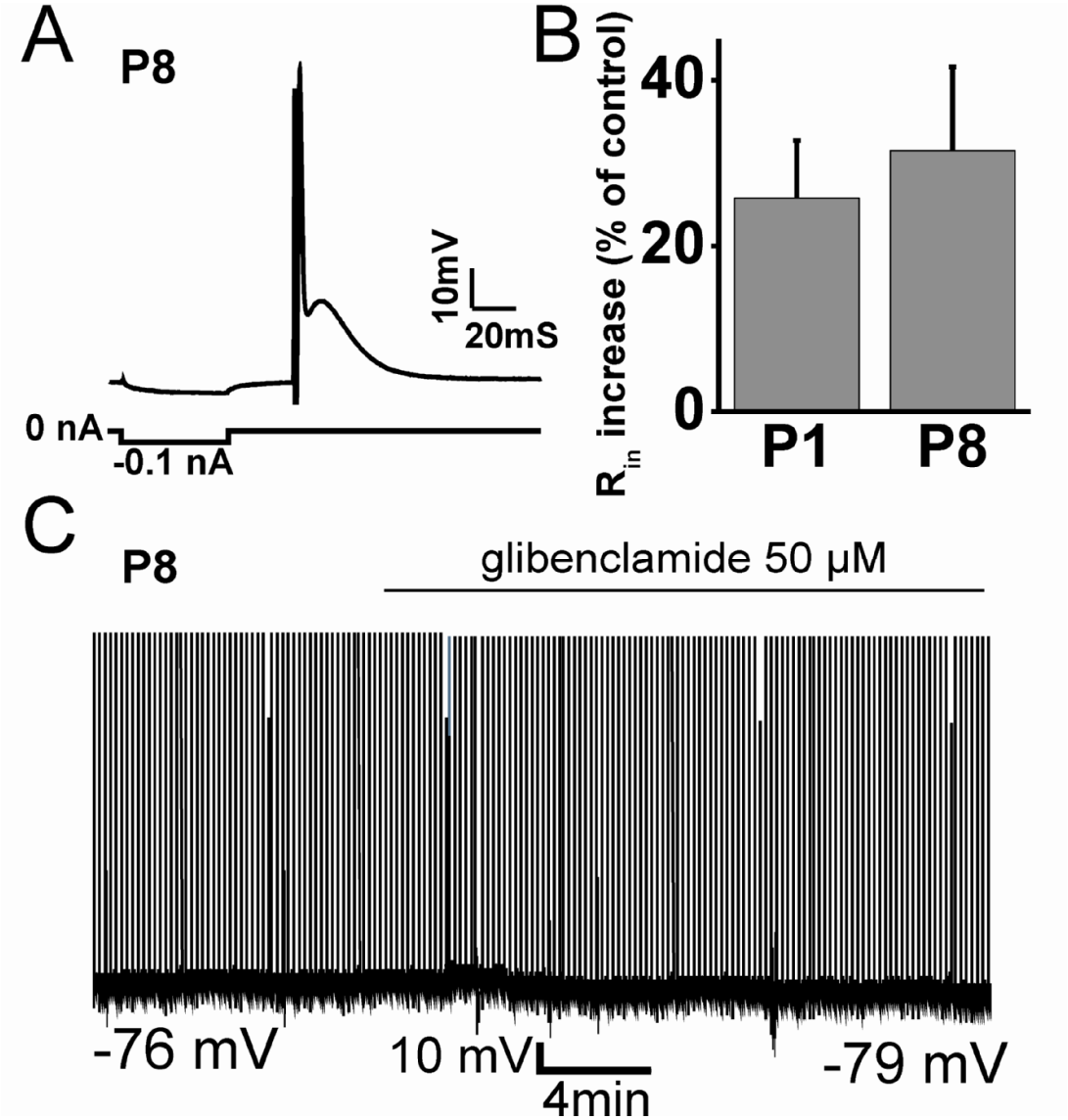

A) Sharp electrode recording from single motoneuron at P8 shows electrotonic potential induced by -0.1 nA pulse to measure input resistance followed by VR stimulus to evoke antidromic spike (truncated). B) Increase in input resistance after application of glibenclamide was not significantly different between P1 and P8. C) Continuous recording from single motoneuron at P8 shows slow membrane hyperpolarization after application of glibenclamide (indicated by the horizontal bar). Large deflections are truncated antidromic spikes. All the experiments were performed in the presence of fast synaptic transmission inhibitors (3 mM kynurenic acid, 20 µM bicuculline, 1 µM strychnine).

3.2. Patch clamp of lumbar motoneurons

Developmental changes in $E_{GABA/Gly}$ may provide useful information for the functional role of CFTR in Cl^- homeostasis. To this end, the blind whole-cell patch clamp method of recording from sagittally hemisected spinal cords was set up (Fig. 7 A). The reason to select patch electrodes was the need to improve the space clamp of motoneurons enabling the observation of the actual reversal of the synaptic currents mediating the spontaneous IPSPs. 3 mM kynurenic acid was used to block of glutamatergic and cholinergic transmission (Hilmas et al 2001; Marchetti et al 2002) to pharmacologically isolate spontaneous synaptic events mediated by GABA and glycine (see example in Fig. 7 B for P1 motoneuron). In fact, such sPSCs disappeared when strychnine (1 μM) and bicuculline (20 μM) were applied (data not shown; Takahashi, 1984). No age-dependent differences in motoneuronal electrophysiological properties were found and the data were, therefore, pooled together (Table 7). The potential value corresponding to 0 net current flow (resting potential) was in the range -75 to -85 mV at P1 and P8. In kynurenic acid solution motoneuron resistance was 118.5±10.4 MΩ (n=21). Antidromically evoked spike amplitude was 95.9±4.4 mV (n=21) Control experiments showed that there was no change in $E_{GABA/Gly}$ after 30 min in kynurenic acid solution alone (Fig. 15 A). However, as it is shown on Fig. 15 B $E_{GABA/Gly}$ were significantly different at P1 and P8 (-73.5±0.8 mV and -79.6±1.1 mV respectively, $p<0.01$, n=13 for P1, n=8 for P8). $E_{GABA/Gly}$ values at P1 and P8 were very similar to those obtained using Renshaw cell-mediated recurrent inhibition recorded with sharp electrodes (Jean-Xavier et al., 2006).

Table 7. Electrophysiological properties of lumbar motoneurons at P1 and P8 derived from patch clamp recordings.

Resting Potential, mV (±SE)	Motoneuron Resistance, MΩ (±SE)	Spike Amplitude, mV (±SE)
-80.2±1.2 (n=21)	118.5±10.4 (n=21)	95.9±4.4 (n=21)

Figure 15. $E_{GABA/Gly}$ in spinal motoneurons.

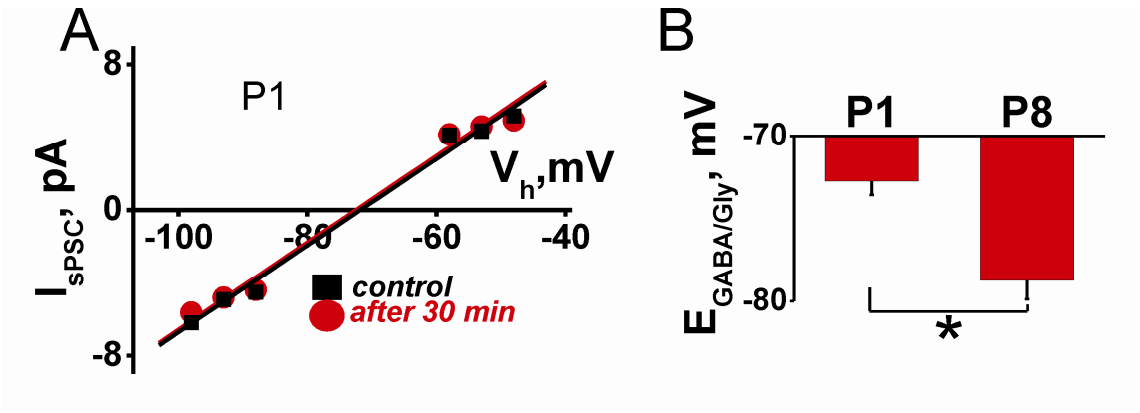

A) Example showing no shift in $E_{GABA/Gly}$ value (obtained from the horizontal intercept) after 30 min in kynurenic acid solution alone in P1. B) Average values of $E_{GABA/Gly}$ recorded at P1 and P8 in control solution (*$p<0.01$, n=13 for P1, n=8 for P8).

3.3. Effect of CFTR and NKCC1 block on $E_{GABA/Gly}$

To test whether CFTR was involved in Cl^- homeostasis, $E_{GABA/Gly}$ before and after glibenclamide application was measured. The data examples of Fig. 16 A show that there was no voltage dependent change (within the -110 and -50 mV range) in the rate of rise of sPSC either in control or after glibenclamide, suggesting that those events were satisfactorily clamped. Fig. 16 B confirms that the decay time was not changed by glibenclamide on the same P1 motoneuron at -95 mV. Interestingly, unlike the data obtained with sharp electrode recording (Fig. 14 B), motoneuron resting resistance measured as the slope of I-V curve was not significantly different in control or after glibenclamide (Fig. 16 C). As demonstrated by the example for P1 motoneuron in Fig. 17 A, I-V plots for synaptic events were compared before and after applying 50 μM glibenclamide to estimate $E_{GABA/Gly}$ values. After 20 min of glibenclamide application, the negative shift in $E_{GABA/Gly}$ value vs control at P1 was 6.0±1.2% ($p<0.01$, $n=5$). The effect of 50 μM glibenclamide on $E_{GABA/Gly}$ at P8 was smaller (2.5±0.5%, $p<0.01$, $n=5$; Fig. 17 B).

Next, it was checked if NKCC1 activity could influence $E_{GABA/Gly}$ values. Application of the NKCC1 blocker bumetanide (10 μM for 20 min; Gonzalez-Islas et al., 2009) made the value of the reversal potential more negative at P1 (6.5±2.5%, $p<0.01$, $n=5$; Fig. 17 B). Conversely, no significant difference was found at P8 (Fig. 17 B). Application of bumetanide didn't produce any change in the basal electrophysiological properties of motoneurons at P1 and P8.

Figure 16. Glibenclamide did not alter rise/decay time and resting I-V curve.

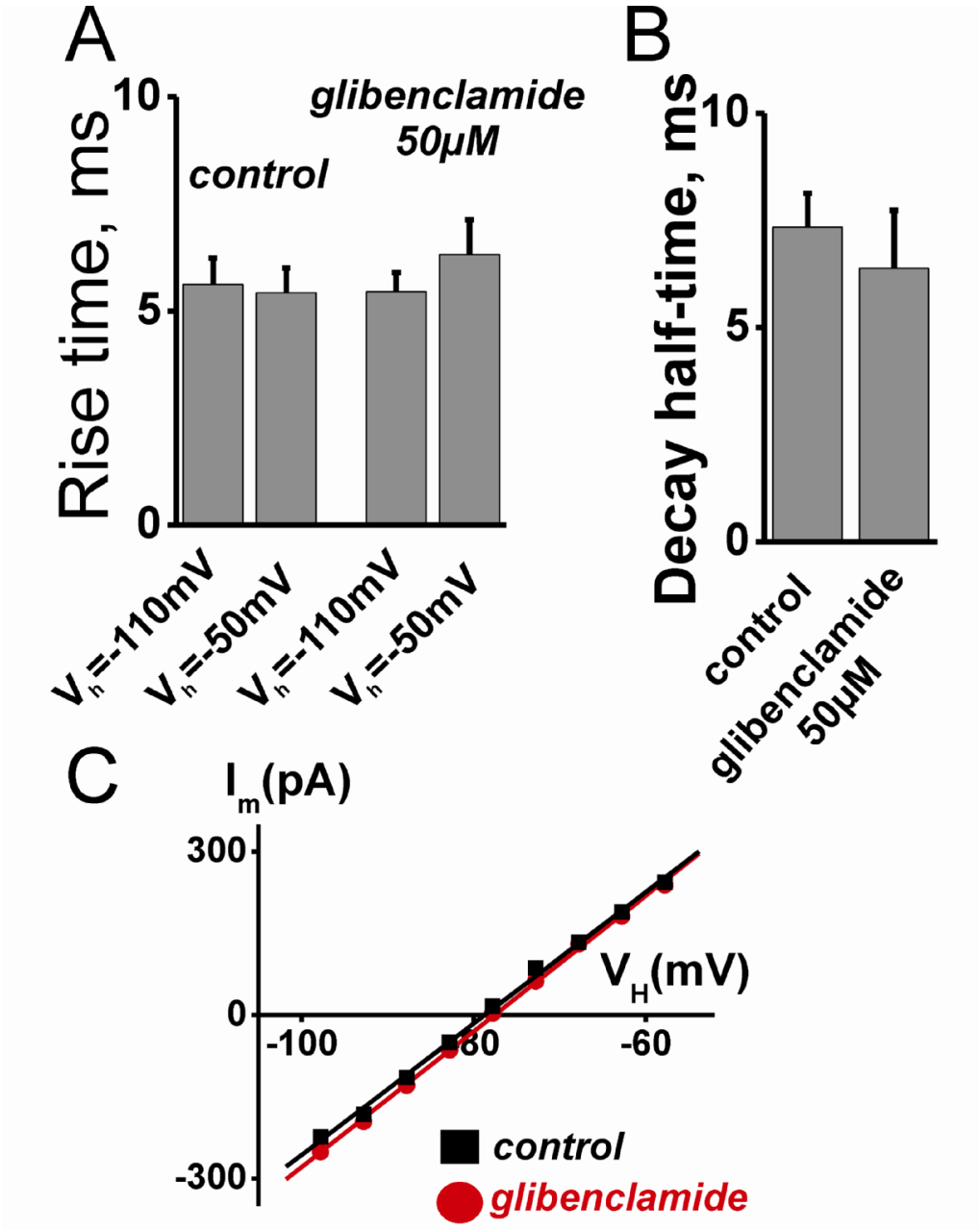

A) Rise time (from 10 to 90 %) measured at different potentials before and after glibenclamide application (example from P1 motoneuron) without significant change. B) Half-decay time (from 90 to 40 %) measured at -95 mV before and after glibenclamide application (from the same P1 example as in A) shows similar values, indicating no apparent alteration in the event (n=20 for this cell) decline. C) Linear character of I-V curve before and after glibenclamide application shows that no voltage activated currents appeared in the range of potentials used.

Figure 17. Effect of glibenclamide and bumetanide on $E_{GABA/Gly}$.

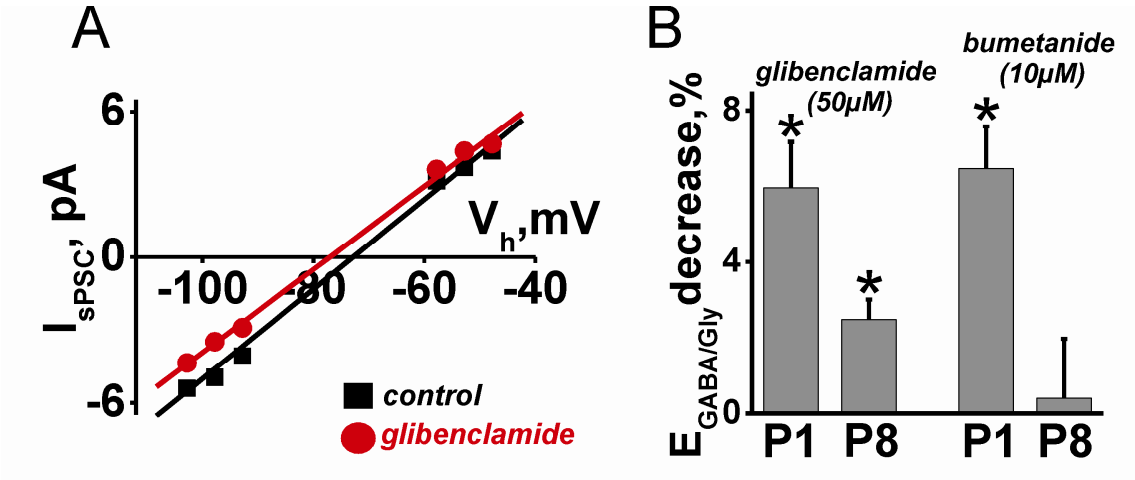

A) Example of the negative shift (-4mV) in $E_{GABA/Gly}$ value (obtained from the horizontal intercept) produced by 50 μM glibenclamide at P1. B) Histograms summarize negative shift in $E_{GABA/Gly}$ expressed as percent of control, produced by either 50 μM glibenclamide or 10 μM of bumetanide at P1 and P8 (*$p<0.01$ from corresponding controls at the same age, n=5).

4. MODELING

It might be argued that the electrophysiological changes induced by glibenclamide were relatively small. Nevertheless, because of the changes in intensity and distribution of CFTR during development, their functional effects on motoneurons could be more important than initially imagined. It was, however, difficult to experimentally measure how discrete alterations in membrane properties were mediated by CFTR distributed to different motoneuron compartments. Thus, to gain some information about this issue, a recent 3D model of the neonatal rat motoneuron (Ostroumov, 2007) was used to study the potential impact of CFTR inhibition on motoneuron excitability and $E_{GABA/Gly}$ by taking

into account the age-dependent expression and distribution of this protein (weaker and mainly somatic at P1 vs stronger and spreading out to dendrites at P8; Fig. 11 C).

4.1. How can CFTR distribution influence motoneuronal input resistance?

In simulations, sharp electrode penetration was mimicked by drastically decreasing the value of the somatic R_m (which is the model variable to replicate alterations in motoneuron conductance) from 5300 $\Omega \cdot cm^2$ (Thurbon et al., 1998) to 600 $\Omega \cdot cm^2$ that corresponded to the input resistance value (calculated from the simulated electrotonic potentials depicted in Fig. 18 A, B; P1 motoneuron) similar to the one detected experimentally (on average 40 MΩ for P1) in control conditions with sharp electrodes. Hence, after setting the model conditions to those observed upon sharp electrode penetration, it was explored, by manipulating R_m values, how, at different ages, motoneuronal input resistance could be changed by glibenclamide. A 30% increase in R_m value restricted to the soma raised the calculated input resistance (by 22.6%) as much as the result observed experimentally at P1 (Fig. 18 C). The experimental results obtained at P8 were mimicked by a 35% R_m increase at the soma as well as in the proximal dendrites (26.9%; Fig. 18 C). Proximal dendrites were modeled as cylindrical segments with their origin on motoneuronal soma and a maximal length of 25 µm (Ostroumov, 2007). Experimental and modeling data therefore concurred to show that, under sharp electrode conditions, CFTR activity likely contributed to the resting input resistance and that its role was not apparently intensified by extending its localization to the proximal dendrites.

Figure 18. Simulations of CFTR influence on motoneuron input resistance in sharp electrode experiments.

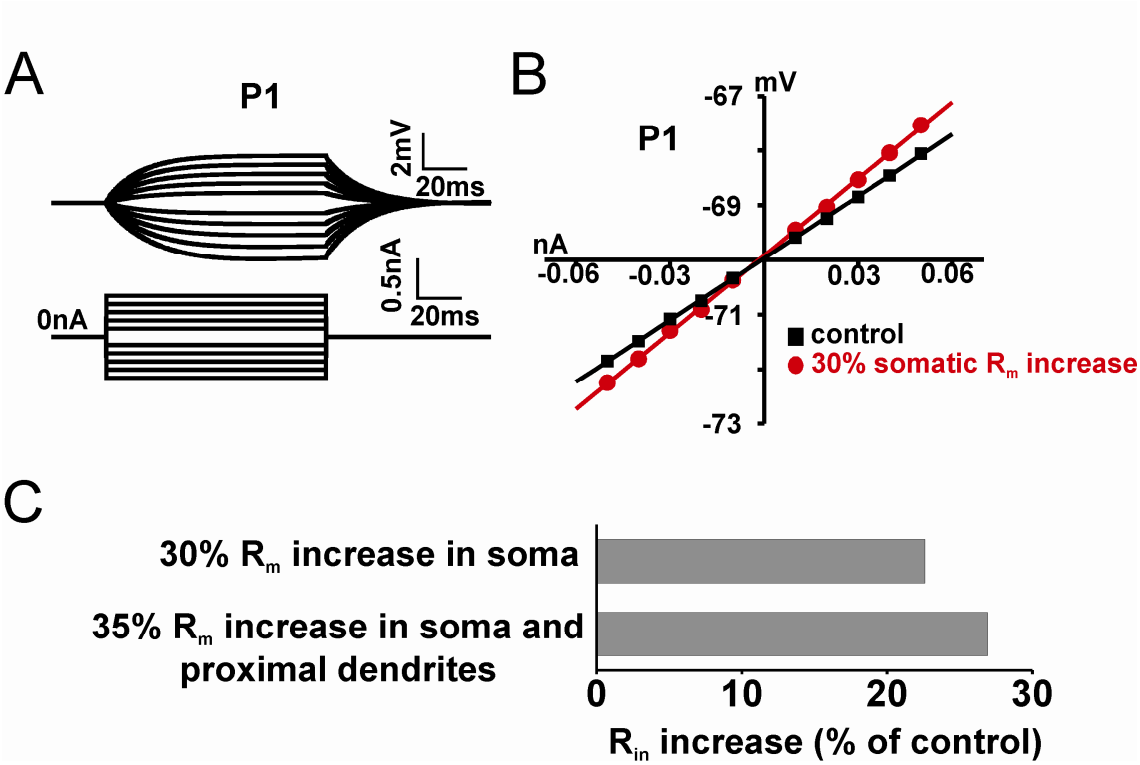

A) Example of voltage responses to currents (0.01 nA step increments in the range from -0.05 to 0.05) injected into the soma of a P1 modeled motoneuron. B) Rise in input resistance (measured as slope of I-V curve) after 30 % increase of the somatic R_m in exemplified P1 motoneuron to mimic the effect of 50 μM glibenclamide. C) Histograms depict the estimated changes in input resistance of P1 motoneuron produced by simulated 30 % increase in somatic R_m. Thirtyfive 35 % increase in R_m at the soma and proximal dendrites of P8 motoneuron produced comparable rise in input resistance like at P1.

4.2. Influence of CFTR inhibition on suprathreshold motoneuron stimulation

The next step was to investigate if, at P1, the 6% shift by glibenclamide of $E_{GABA/Gly}$ could be important for the excitability of motoneurons. To study this issue the AP initiation with a recurrent IPSP were paired (Fig. 19; see methods) after setting the $E_{GABA/Gly}$ value at -60 mV, i.e. with a 10 mV driving force as observed experimentally at P1. The motoneuron resting potential was always assumed to be -70 mV throughout.

In control conditions simulated for a P1 motoneuron, 0.4 nA depolarizing step generated an AP (Fig. 19) that, when paired with the recurrent IPSP, required a larger (0.5 nA) depolarizing step to be reproduced again. However, a 6% negative shift of $E_{GABA/Gly}$ as experimentally observed with glibenclamide led to spike failure when the AP (evoked by 0.5 nA) was paired with the IPSP (Fig. 19 A), although the AP could be reinstated by increasing the amplitude of the depolarizing step to 0.7 nA (not shown). Then it was checked if the smaller effect of glibenclamide on $E_{GABA/Gly}$ observed experimentally in P8 animals was still important for the excitability of motoneurons. Simulating a 2.5% negative shift in $E_{GABA/Gly}$ together with 4 mV driving force at P8 was tested with the model: even such a slight change was critical for suppressing AP initiation (Fig. 19 B).

Figure 19. Example of modeling the interaction between suprathreshold depolarizing step evoking an AP and the recurrent IPSP.

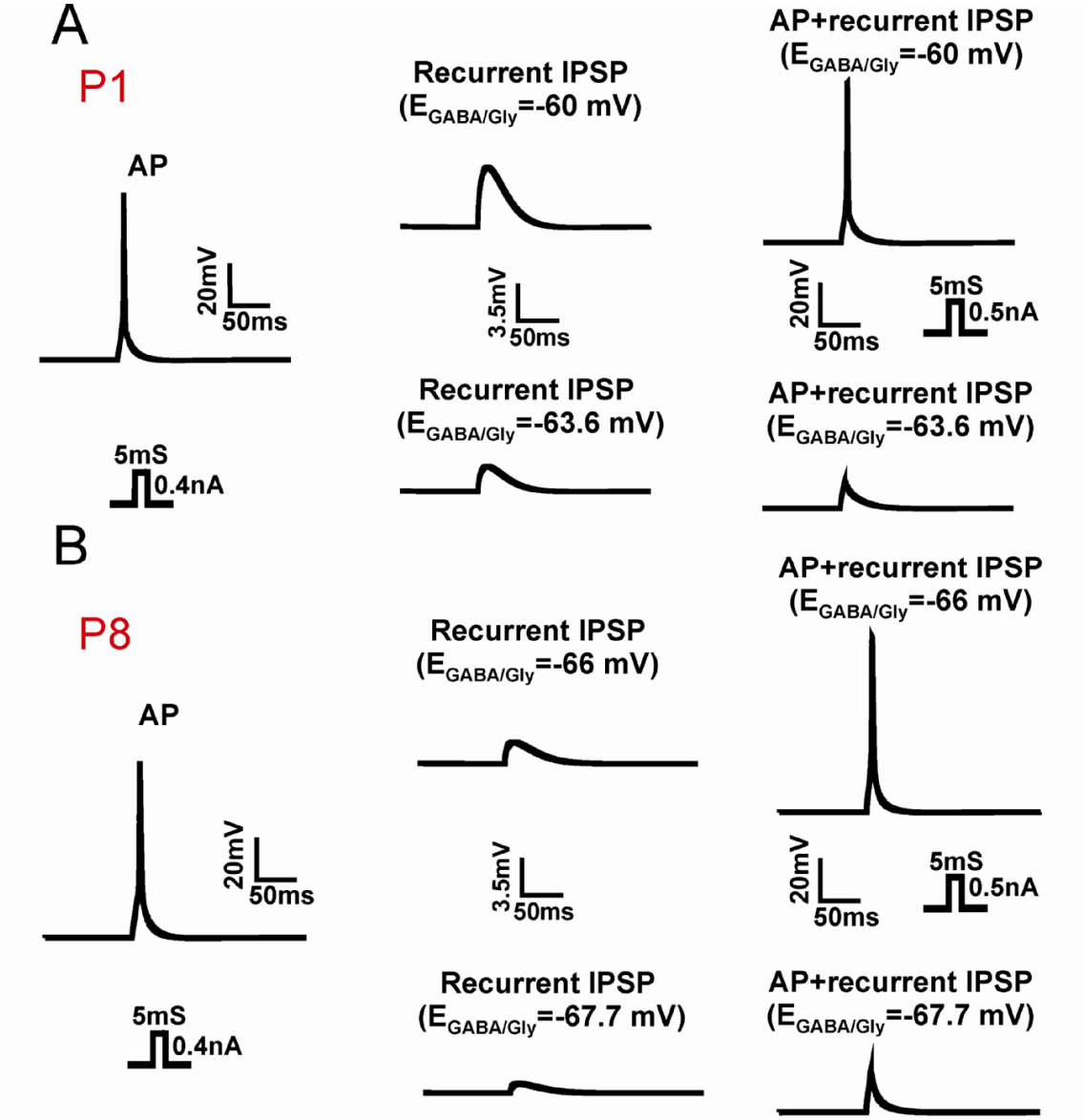

A) IPSP is depolarizing because the $E_{GABA/Gly}$ is set positive to the -70 mV resting potential for P1 modeled motoneuron. To replicate the AP when the two events coincided, it was necessary to raise the stimulus intensity to 0.5 from 0.4 nA, indicating that the IPSP could depress spike generation in control conditions. Six % negative shift in $E_{GABA/Gly}$ produced a smaller amplitude IPSP and led to spike failure when tested with 0.5 nA, suggesting further elevation in the spike threshold. B) The same as in A) but for P8 modeled cell. In this case 2.5 % negative shift in $E_{GABA/Gly}$ and 4 mV driving force for IPSP were introduced.

4.3. Influence of CFTR inhibition on subthreshold motoneuron stimulation

Starting from the same resting potential (-70 mV), it was next investigated the interaction between an EPSP subthreshold for AP generation and the IPSP in order to find out if the depolarizing nature of the IPSP could summate with the EPSP to produce an excitatory or inhibitory action. In accordance with the modeling data by Jean-Xavier et al. (2007), simulating coincidence in the onset of the EPSP and IPSP failed to generate an AP, in keeping with the inhibitory nature of the IPSP. However, the precise time-coincidence of such events is probably an unusual phenomenon. Hence, it was investigated what would occur to motoneuron excitability when, at P1, the EPSP was timed to be produced on the decay phase of the IPSP (Fig. 20): in this case an AP appeared. Introducing a 6% negative shift of $E_{GABA/Gly}$, as observed after glibenclamide application, prevented the EPSP from firing an AP during the IPSP decay (Fig. 20 A). The same result was obtained by modeling a P8 motoneuron when the $E_{GABA/Gly}$ driving force was set to be 4 mV and the change in $E_{GABA/Gly}$ evoked by glibenclamide was just 2.5 % (Fig. 20 B). These results suggest that CFTR might play an important role in motoneuron excitability immediately after birth and one week later.

Figure 20. Example of modeling the interaction between subthreshold EPSP and recurrent IPSP for P1 modeled motoneuron.

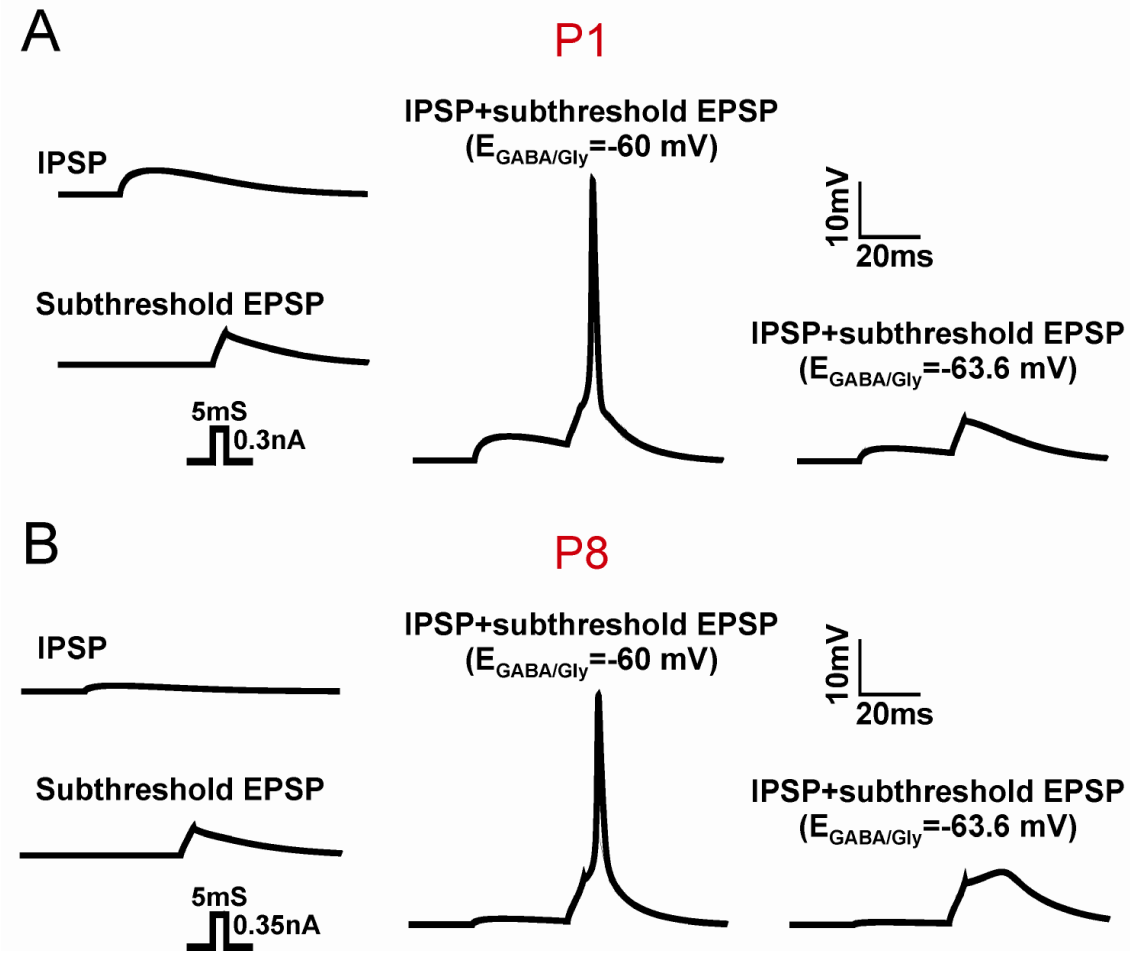

A) The EPSP could summate with the IPSP to induce an AP at P1 if the EPSP was timed to occur on the decay phase of the IPSP. However, with the temporal occurrence of IPSP and EPSP as before, a 6 % negative shift in $E_{GABA/Gly}$ prevented AP initiation. Resting potential was assumed to be -70 mV. B) For P8 modeled cell 2.5 % negative shift in $E_{GABA/Gly}$ and 4 mV driving force for IPSP were introduced.

DISCUSSION

The principal finding of the present Ph.D. project is the novel characterization of the time profile of CFTR gene expression and immunohistochemical localization in the neonatal rat spinal cord during the first postnatal week with consequential influence on $E_{GABA/Gly}$ values and excitability of motoneurons. These observations suggest that, in addition to KCC2 and NKCC1, CFTR was a functional (yet so far neglected) contributor to Cl^- homeostasis and, with the help of modeling, it was possible to estimate its impact on motoneurons.

Gene expression profile of Cl^- transporters in the developing rat spinal cord

Real time RT-PCR experiments gave an opportunity to monitor developmental changes in CFTR, NKCC1 and KCC2 gene expression, a result not available to date despite detailed investigations into the developmental role of the transporters NKCC1 and KCC2 (Plotkin et al., 1997b; Stein et al., 2004). A gender difference for KCC2 gene expression was observed that was higher in female tissue both at P1 and P8. Since KCC2 is neuron-specific (Payne et al., 1996), and the number of neurons is reportedly higher in male spinal tissue (for review see Forger, 2009; see also stronger β-tubulin III signal in Fig. 8 B), it seems likely that the difference between male and female KCC2 gene expression was not due to the different number of neurons. Although the physiological role of this sexual dimorphism remains to be determined, on the basis of the present observations records of male and female data were kept separate. It was also interesting if postnatal

sex differences in the expression of Cl^- transporters might partly contribute to the discrepancies reported in the literature for the developmental changes in $E_{GABA/Gly}$ for males and females (Galanopoulou et al., 2003; Nuñez and McCarthy, 2007; Perrot-Sinal et al., 2007).

In the present study, the activity of all genes under investigation showed a significant age-related rise for both genders. The increase in KCC2 mRNA accords with the notion that the developmental up-regulation of KCC2 is responsible for the shift from depolarizing to hyperpolarizing GABAergic responses (DeFazio et al., 2000; Rivera et al., 1999; Stil et al., 2009). Present results also provided a first description of changes in the NKCC1 gene expression during the first postnatal week. Despite its proposed role in Cl^- homeostasis, the current lack of an NKCC1 antibody suitable for immunocytochemistry or western blot analysis (Blaesse et al., 2009) has seriously hampered direct validation of this proposal. Thus, RT PCR data indicated that, at least at mRNA level, there was a strong growth in NKCC1 and that it was clearly correlated with the growth in CFTR signal. Such a correlation was not detected between NKCC1 and KCC2. Hence, shifts in Cl^- homeostasis could not simply be explained by a diametrically-opposed change in NKCC1 vs KCC2 and required looking for additional proteins like CFTR.

CFTR signal in the developing rat spinal cord

The CFTR gene activity was present in rat lumbar spinal cord already at P1 and gradually increased up to P8. Immunohistochemistry data validated the CFTR protein location in

the same tissue at P1 and P8. In particular, CFTR was expressed in large ventral horn cells, presumably motoneurons because of their size, laminar distribution and immunopositivity to the neuron marker Map-2. The present study does not exclude that this protein is also expressed by other spinal cells, as CFTR has recently been observed even in human spinal cord interneurons (Guo et al., 2009). In the rat spinal cord at the end of the first postnatal week, CFTR protein expression became more evident in neuronal processes and somata, prompting further experiments to explore its function.

Using glibenclamide to probe the role of CFTR

In accordance with the former investigation (Ostroumov et al., 2007), the sulphonylurea glibenclamide at the concentration of 50 μM was used to inhibit CFTR function. While glibenclamide was developed as a K_{ATP} channel blocker to treat diabetes (Mironov et al., 1998), at μM concentrations it is a canonical inhibitor of CFTR (Schultz et al., 1999). A recent report has found no effect of glibenclamide on rat spinal motoneurons compatible with pharmacological block of K_{ATP} channels (Ostroumov et al., 2007). Furthermore, effects identical to those of glibenclamide are observed after applying tolbutamide and diphenylamine-2,2'-dicarboxylic acid (DPC), both considered to be CFTR inhibitors (Schultz et al., 1999). In the present study, the action of glibenclamide was exploited to check the CFTR function on $E_{GABA/Gly}$ and basic motoneuron properties immediately after birth and at the end of the first postnatal week. Since enhanced Cl^- permeability has been shown to mediate the synaptic action of GABA and glycine on spinal motoneurons (Cupello, 2003; Hamill et al., 1983; Wu et al., 1992), and there is no apparent role for

HCO_3^- (Jean-Xavier et al., 2006), the effect of glibenclamide on $E_{GABA/Gly}$ was taken as an index of the CFTR involvement in motoneuronal Cl^- homeostasis.

Glibenclamide actions on passive membrane properties of motoneurons

Using sharp-electrodes for investigating reversal potentials has the important limitation of the inherently low current passing ability that prevents considerable shifts in holding potential to achieve effective space clamp of synaptic events. On the other hand, it was possible to minimize alterations in intracellular milieu due to patch electrode dialysis and, therefore, to check any role of CFTR on basic membrane properties under current clamp conditions. Glibenclamide produced motoneuron resistance increase and membrane hyperpolarization consistent with the inhibition of a background outward conductance that was comparatively similar at P1 and P8. Previous investigation has shown changes in passive membrane motoneuron properties produced by glibenclamide to be readily accounted by inhibition of a CFTR-dependent background conductance (Ostroumov 2007; Ostroumov et al., 2007). Assuming that this effect of glibenclamide is due to inhibition of CFTR which is already largely expressed at somatic level of motoneurons even at P1, it may be suggested that there is a CFTR-modulated leak inward conductance that regulates the basic somatic properties. Although a possible candidate for rat spinal neurons is a cAMP-activated Cl^- conductance (Ostroumov et al., 2007), further studies are necessary to identify this mechanism. It was, however, interesting that whole-cell patch clamp conditions did not allow observing the resistance rise produced by

glibenclamide, suggesting perhaps that intracellular dialysis had washed away the soluble mediator(s) of such an effect.

Changes in $E_{GABA/Gly}$ in relation to E_{Cl}

The whole cell patch-clamp technique allowed to investigate changes in synaptic event reversal before and after application of glibenclamide. In the presence of kynurenic acid to suppress ionotropic glutamate receptor and nicotinic cholinergic events (Hilmas et al., 2001; Marchetti et al., 2002), $E_{GABA/Gly}$ of synaptic currents was recorded, a parameter that provides a reliable index of Cl^- concentration at the synaptic level (Gonzalez-Islas et al., 2009). $E_{GABA/Gly}$ values at P1 and P8 were very similar to those obtained using Renshaw cell-mediated recurrent inhibition recorded with sharp electrodes (Jean-Xavier et al., 2006). It is noteworthy that the $E_{GABA/Gly}$ was less negative at P1 (-73.5±0.8 mV) than at P8 (-79.6±1.1 mV), and that, in either case, such a value was more negative than the E_{Cl} calculated with the Nernst equation. The discrepancy between calculated E_{Cl} and measured $E_{GABA/Gly}$ in the spinal cord has already been reported by Gonzalez-Islas et al. (2009) and Jean-Xavier et al. (2006). One parsimonious interpretation is that the intracellular Cl^- concentration was kept at a relatively low level by a continuous extrusion, probably due to the operation of KCC2 that was already expressed at birth as shown in the present study.

Changes in $E_{GABA/Gly}$ evoked by glibenclamide

Glibenclamide produced a negative shift in $E_{GABA/Gly}$ which was smaller at the end of first postnatal week. These changes were not accompanied by significant alterations in the rate of rise of the synaptic currents, suggesting that there was no inhibition by glibenclamide of transmitter release, or alteration in the space clamp properties. Likewise, the similar decay time of synaptic events before and after glibenclamide application indicated that partial block by this drug of the open Cl^- channels was unlikely.

Since CFTR is a known regulator of membrane conductances (Kunzelmann and Schreiber, 1999) and, apparently, of NKCC1 in the spinal cord (Ostroumov et al., 2007), the present result could be explained by assuming a triad arrangement concerning the Cl^- transport process. Thus, on the one hand, KCC2 would operate to extrude Cl^- (DeFazio et al., 2000; Rivera et al., 1999; Stein et al., 2004), NKCC1 would counteract it by pumping this anion in (Plotkin et al., 1997b; Yamada et al., 2004), and CFTR would be a positive regulator of the latter mechanism (Fig.21). By inhibiting CFTR, this equilibrium might have been perturbed when NKCC1 is allegedly most active, namely at birth (Yamada et al., 2004). Indeed, a low concentration of bumetanide, which is reported to be a selective blocker of NKCC1 (Gonzalez-Islas et al., 2009), could significantly shift $E_{GABA/Gly}$ only at P1.

Previous investigations have indicated a close inter-relationship between CFTR and NKCC1 because, in epithelial cell cultures, CFTR stimulates NKCC1 to increase intracellular Cl^- (Adam et al., 2005), as well as to enhance the functional expression of this transporter (Shumaker and Soleimani, 1999). On the basis of the present data it is

proposed that CFTR exerted its modulatory role on NKCC1 activity via intracellular signaling pathways, whose identity in spinal motoneurons is currently unknown, but their role via phosphorylation has been previously inferred in fibroblasts (Stutts et al., 1997).

The reason for the gradual loss of NKCC1 contribution to $E_{GABA/Gly}$ during the first week of life is unclear, and cannot be attributed to poor expression of CFTR or impaired NKCC1 gene expression that actually grew with age, perhaps in cells other than motoneurons. CFTR protein expression was increased in motoneurons during the first week (Fig. 21) and its effect on the cell input resistance was still substantial at P8, whereas the contribution to $E_{GABA/Gly}$ was decreased with the development. These data suggest the breakdown of functional association between CFTR and NKCC1 at the end of the first postnatal week, despite of high correlation in the developmental expression of these two genes.

Figure 21. Developmentally regulated functional expression of KCC2, NKCC1 and CFTR determines chloride transmembrane gradient during maturation.

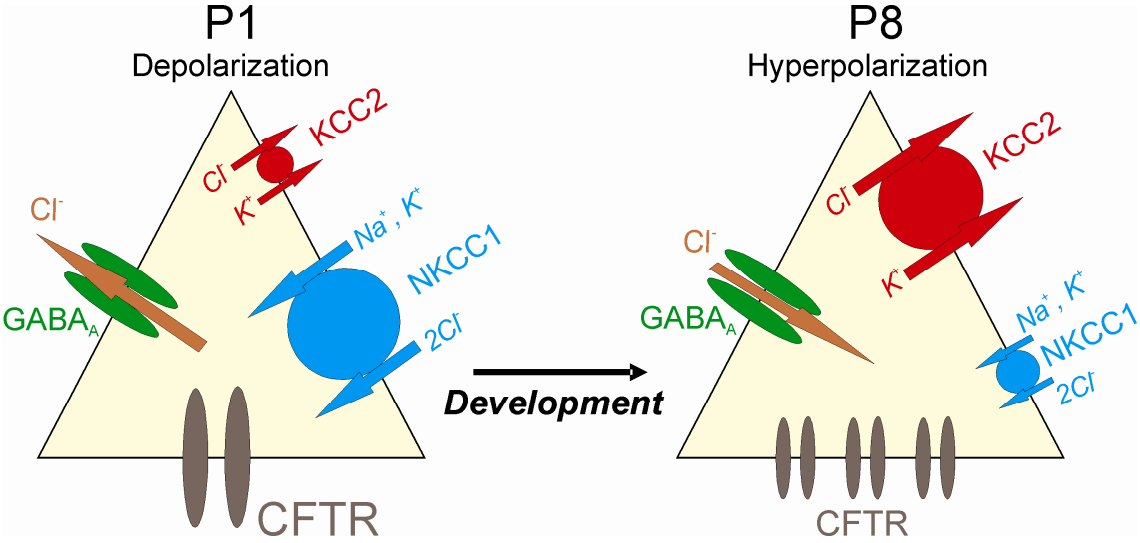

Revised version of Figure 2 by taking into account the present data that include CFTR as a possible regulator of NKCC1. CFTR influences Cl^- homeostasis mainly at birth, whereas this functional property of this protein becomes weaker at the end of the first postnatal week. However, the expression of CFTR protein is growing during postnatal development (note the increased number of CFTR symbols at P8 on the scheme)

Estimating the potential impact of CFTR on Cl^- mediated synaptic events and its functional implication

On motoneurons, changes in $E_{GABA/Gly}$ evoked by glibenclamide were comparatively small. Nonetheless, even small variations in $E_{GABA/Gly}$ might be critical for inhibition of such cells (Jean-Xavier et al., 2007). The present study tested this possibility by using a 3D model of the neonatal rat motoneuron more advanced that the standard simplified cable model (Ostroumov, 2007). With such a tool, it was first observed that, in control

conditions, the depolarizing IPSP consistently raised the threshold for generating an AP, indicating that the IPSP had a functional inhibitory action on motoneurons.

The 6 % change in $E_{GABA/Gly}$ produced by glibenclamide at P1, together with the smaller amplitude of the depolarizing IPSP, depressed the AP generation more strongly than in control. This effect was observed at P8 as well, although the action of glibenclamide was accompanied by an even smaller alteration in $E_{GABA/Gly}$ (2.5 %).

These simulations together with the experimental results suggest that, on neonatal rat spinal motoneurons, GABA/glycine mediated synaptic depolarizations depressed firing probably via the underlying Cl^- conductance shunt rather than via changes in the membrane potential near AP threshold. Nevertheless, in control conditions, the IPSP inhibitory function was transient because a simulated local depolarization (such as an EPSP) could summate with the IPSP and trigger a spike when the EPSP occurred during the falling phase of the IPSP characterized by fading of its inhibitory conductance together with electrotonic dissipation of the underlying potential change (Jean-Xavier et al., 2007). When glibenclamide made the $E_{GABA/Gly}$ value more negative, the IPSP amplitude was smaller and less effective in summating with the late-onset EPSP to reach threshold, thus yielding AP suppression. These observations accord with the dual functional nature of the depolarizing IPSP in the spinal cord of the developing rat (Jean-Xavier et al., 2007) and highlight the novel contribution by CFTR to this phenomenon hitherto underestimated.

In conclusion, RT PCR and immunohistochemistry techniques showed that CFTR was expressed in motoneurons of the rat lumbar spinal cord during the first postnatal week. Electrophysiological recordings with the sharp electrodes demonstrated this protein to be

functional in P1-P8 motoneurons. Whole cell patch-clamping of spinal motoneurons confirmed the hypothesis, made at the beginning of this study, namely that CFTR was involved in Cl^- homeostasis mediating GABAergic and glycinergic events in a developmentally-regulated fashion. The present results support the project hypothesis that CFTR regulated NKCC1 activity at an early stage of postnatal development and that this interaction resulted in the modulation of Cl^- mediated synaptic currents. Future studies will be necessary to identify the precise molecular mechanisms through which CFTR contributes to Cl^- regulation.

REFERENCES

Adam G, Ousingsawat J, Schreiber R, Kunzelmann K (2005) Increase in intracellular Cl^- concentration by cAMP- and Ca^{2+}-dependent stimulation of M1 collecting duct cells. Pflugers Arch 449:470–478.

Aguado F, Carmona MA, Pozas E, Aguiló A, Martínez-Guijarro FJ, Alcantara S, Borrell V, Yuste R, Ibañez CF, Soriano E (2003) BDNF regulates spontaneous correlated activity at early developmental stages by increasing synaptogenesis and expression of the K^+/Cl^- co-transporter KCC2. Development 130:1267-1280.

Aoyama K, Watabe M, Nakaki T (2008) Regulation of neuronal glutathione synthesis. J Pharmacol Sci 108:227-238.

Balakrishnan V, Becker M, Lohrke S, Nothwang HG, Guresir E, Friauf E (2003) Expression and function of chloride transporters during development of inhibitory neurotransmission in the auditory brainstem. J Neurosci 23:4134–4145.

Ben-Ari Y (2002) Excitatory actions of GABA during development: the nature of the nurture. Nat Rev Neurosci 3:728-739

Ben-Ari Y, Gaiarsa JL, Tyzio R, Khazipov R (2007) GABA: a pioneer transmitter that excites immature neurons and generates primitive oscillations. Physiol Rev 87:1215-1284.

Bennett MR, McGrath PA, Davey DF, Hutchinson I (1983) Death of motorneurons during the postnatal loss of polyneuronal innervation of rat muscles. J Comp Neurol 218:351–363.

Blaesse P, Airaksinen MS, Rivera C, Kaila K (2009) Cation-chloride cotransporters and neuronal function. Neuron 61:820-838.

Blaesse P, Guillemin I, Schindler J, Schweizer M, Delpire E, Khiroug L, Friauf E, Nothwang HG (2006) Oligomerization of KCC2 correlates with development of inhibitory neurotransmission. J Neurosci 26:10407-10419

Boulenguez P, Liabeuf S, Bos R, Bras H, Jean-Xavier C, Brocard C, Stil A, Darbon P, Cattaert D, Delpire E, Marsala M, Vinay L (2010) Down-regulation of the potassium-chloride cotransporter KCC2 contributes to spasticity after spinal cord injury. Nat Med 16:302-307

Cavalier SJ, Gambetti P (1981) Dystrophic axons and spinal cord demyelination in cystic fibrosis. Neurology 31:714-718.

Cherubini E, Gaiarsa JL, Ben-Ari Y (1991) GABA: an excitatory transmitter in early postnatal life. Trends Neurosci 14:515-519.

Clayton GH, Owens GC, Wolff JS, Smith RL (1998) Ontogeny of cation-Cl^- cotransporter expression in rat neocortex. Brain Res Dev Brain Res 109:281-292.

Cohen I, Navarro V, Clemenceau S, Baulac M, Miles R (2002) On the origin of interictal activity in human temporal lobe epilepsy in vitro. Science 298:1418-1421.

Coull JA, Boudreau D, Bachand K, Prescott SA, Nault F, Sík A, De Koninck P, De Koninck Y (2003) Trans-synaptic shift in anion gradient in spinal lamina I neurons as a mechanism of neuropathic pain. Nature 424:938-942.

Cupello A (2003) Neuronal transmembrane chloride electrochemical gradient: a key player in $GABA_A$ receptor activation physiological effect. Amino Acids 24:335–346.

DeFazio RA, Keros S, Quick MW, Hablitz JJ (2000) Potassium-coupled chloride cotransport controls intracellular chloride in rat neocortical pyramidal neurons. J Neurosci 20:8069-8076.

Delpire E (2000) Cation-chloride cotransporters in neuronal communication. News Physiol Sci 15:309-312.

Delpire E, Lu J, England R, Dull C, Thorne T (1999) Deafness and imbalance associated with inactivation of the secretory Na-K-2Cl co-transporter. Nat Genet 22:192-195.

Delpy A, Allain AE, Meyrand P, Branchereau P (2008) NKCC1 cotransporter inactivation underlies embryonic development of chloride-mediated inhibition in mouse spinal motoneuron. J Physiol 586:1059-1075.

Di A, Brown ME, Deriy LV, Li C, Szeto FL, Chen Y, Huang P, Tong J, Naren AP, Bindokas V, Palfrey HC, Nelson DJ (2006) CFTR regulates phagosome acidification in macrophages and alters bactericidal activity. Nat Cell Biol 8:933–944.

Díez-Guerra FJ, Avila J (1993) MAP2 phosphorylation parallels dendrite arborization in hippocampal neurones in culture. Neuroreport 4:419-422.

Eccles JC (1964) The physiology of synapses. Berlin: Springer.

Egan M, Flotte T, Afione S, Solow R, Zeitlin PL, Carter BJ, Guggino WB (1992) Defective regulation of outwardly rectifying Cl^- channels by protein kinase A corrected by insertion of CFTR. Nature 358:581–584.

Eins S, Spoerri PE, Heyder E (1983) GABA or sodium-bromide-induced plasticity of neurites of mouse neuroblastoma cells in culture. A quantitative study. Cell Tissue Res 229:457-460.

Flagella M, Clarke LL, Miller ML, Erway LC, Giannella RA, Andringa A, Gawenis LR, Kramer J, Duffy JJ, Doetschman T, Lorenz JN, Yamoah EN, Cardell EL, Shull GE (1999) Mice lacking the basolateral Na-K-2Cl cotransporter have impaired epithelial chloride secretion and are profoundly deaf. J Biol Chem 274:26946-26955.

Fonknechten N, Chelly J, Lepercq J, Kahn A, Kaplan JC, Kitzis A, Chomel JC (1992) CFTR illegitimate transcription in lymphoid cells: quantification and applications to the investigation of pathological transcripts. Hum Genet 88:508–512.

Forger NG (2009) The organizational hypothesis and final common pathways: Sexual differentiation of the spinal cord and peripheral nervous system. Horm Behav 55:605-610.

Fulton BP, Walton K (1986) Electrophysiological properties of neonatal rat motoneurones studied in vitro. J Physiol 370:651-678.

Gabriel SE, Clarke LL, Boucher RC, Stutts MJ (1993) CFTR and outward rectifying chloride channels are distinct proteins with a regulatory relationship. Nature 363:263-268.

Galanopoulou AS, Kyrozis A, Claudio OI, Stanton PK, Moshé SL (2003) Sex-specific KCC2 expression and $GABA_A$ receptor function in rat substantia nigra. Exp Neurol 183:628-637.

Gao BX, Ziskind-Conhaim L (1995) Development of glycine- and GABA-gated currents in rat spinal motoneurons. J Neurophysiol 74:113-121.

Gerelsaikhan T, Turner RJ (2000) Transmembrane topology of the secretory Na+-K+-2Cl- cotransporter NKCC1 studied by in vitro translation. J Biol Chem 275:40471-40477.

Gonzalez-Islas C, Chub N, Wenner P (2009) NKCC1 and AE3 appear to accumulate chloride in embryonic motoneurons. J Neurophysiol 101:507-518.

Goldstein AB, Goldstein LS, Perl MK, Haug MT, Arroliga AC, Stillwell PC (2000) Cystic fibrosis patients with and without central nervous system complications following lung transplantation. Pediatr Pulmonol 30:203–206.

Goulding M (2009) Circuits controlling vertebrate locomotion: moving to a new direction. Nat Rev Neurosci 10:507-518.

Guo Y, Su M, Su M, McNutt MA, Gu J (2009) Expression and distribution of cystic fibrosis transmembrane conductance regulator in neurons of the spinal cord. J Neurosci Res 87:3611-3619.

Haas M, Forbush B 3rd The Na-K-Cl cotransporter of secretory epithelia. Annu Rev Physiol 62:515-534.

Hamill OP, Bormann J, Sakmann B (1983) Activation of multiple-conductance state chloride channels in spinal neurones by glycine and GABA. Nature 305:805–808.

Hanrahan J, Gentzsch M, Riordan J (2002) The Cystic Fibrosis Transmembrane Conductance Regulator (ABCC7). In: Holland IB (eds). *ABC Proteins: From Bacteria to Man.* Elsevier Science Ltd. 589-618.

Hasbargen T, Ahmed MM, Miranpuri G, Li L, Kahle KT, Resnick D, Sun D (2010) Role of NKCC1 and KCC2 in the development of chronic neuropathic pain following spinal cord injury. Ann N Y Acad Sci 1198:168-172.

Hasegawa H, Skach W, Baker O, Calayag MC, Lingappa V, Verkman AS (1992) A multifunctional aqueous channel formed by CFTR. Science 258:1477–1479.

Hernandes MS, Troncone LR (2009) Glycine as a neurotransmitter in the forebrain: a short review. J Neural Transm 116:1551-1560.

Hilmas C, Pereira EF, Alkondon M, Rassoulpour A, Schwarcz R, Albuquerque EX (2001) The brain metabolite kynurenic acid inhibits alpha7 nicotinic receptor activity and

increases non-alpha7 nicotinic receptor expression: physiopathological implications. J Neurosci 21:7463-7473.

Hines ML, Carnevale NT (1997) The NEURON simulation environment. Neural Comput 9:1179–1209.

Holmgren CD, Mukhtarov M, Malkov AE, Popova IY, Bregestovski P, Zilberter Y (2010) Energy substrate availability as a determinant of neuronal resting potential, GABA signaling and spontaneous network activity in the neonatal cortex in vitro. J Neurochem 112:900-912.

Hübner CA, Stein V, Hermans-Borgmeyer I, Meyer T, Ballanyi K, Jentsch TJ (2001) Disruption of KCC2 reveals an essential role of K-Cl cotransport already in early synaptic inhibition. Neuron 30:515-524.

Ishiguro H, Steward MC, Naruse S, Ko SB, Goto H, Case RM, Kondo T, Yamamoto A (2009) CFTR functions as a bicarbonate channel in pancreatic duct cells. J Gen Physiol 133:315-326.

Jean-Xavier C, Mentis GZ, O'Donovan MJ, Cattaert D, Vinay L (2007) Dual personality of GABA/glycine-mediated depolarizations in immature spinal cord. Proc Natl Acad Sci U S A 104:11477-11482.

Jean-Xavier C, Pflieger JF, Liabeuf S, Vinay L (2006) Inhibitory postsynaptic potentials in lumbar motoneurons remain depolarizing after neonatal spinal cord transection in the rat. J Neurophysiol 96:2274-2281.

Kaila K, Voipio J (1987) Postsynaptic fall in intracellular pH induced by GABA-activated bicarbonate conductance. Nature 330:163-165.

Kaila K, Voipio J, Paalasmaa P, Pasternack M, Deisz RA (1993) The role of bicarbonate in $GABA_A$ receptor-mediated IPSPs of rat neocortical neurones. J Physiol 464:273-289.

Kaplan MR, Plotkin MD, Lee WS, Xu ZC, Lytton J, Hebert SC (1996) Apical localization of the Na-K-Cl cotransporter, rBSC1, on rat thick ascending limbs. Kidney Int 49:40-47.

Kartner N, Augustinas O, Jensen TJ, Naismith AL, Riordan JR (1992) Mislocalization of delta F508 CFTR in cystic fibrosis sweat gland. Nat Genet 1:321-327.

Katchman AN, Vicini S, Hershkowitz N (1994) Mechanism of early anoxia-induced suppression of the $GABA_A$-mediated inhibitory postsynaptic current. J Neurophysiol 71:1128-1138.

Kelsch W, Hormuzdi S, Straube E, Lewen A, Monyer H, Misgeld U (2001) Insulin-like growth factor 1 and a cytosolic tyrosine kinase activate chloride outward transport during maturation of hippocampal neurons. J Neurosci 21:8339-8347.

Khirug S, Huttu K, Ludwig A, Smirnov S, Voipio J, Rivera C, Kaila K, Khiroug L (2005) Distinct properties of functional KCC2 expression in immature mouse hippocampal neurons in culture and in acute slices. Eur J Neurosci 21:899-904.

Khirug S, Yamada J, Afzalov R, Voipio J, Khiroug L, Kaila K (2008) GABAergic depolarization of the axon initial segment in cortical principal neurons is caused by the Na-K-2Cl cotransporter NKCC1. J Neurosci 28:4635-4639.

Kiehn O (2006) Locomotor circuits in the mammalian spinal cord. Annu Rev Neurosci 29:279-306.

Kunzelmann K, Schreiber R (1999) CFTR, a regulator of channels. J Membr Biol 168(1):1-8.

Kuzhandaivel A, Margaryan G, Nistri A, Mladinic M (2010) Extensive glial apoptosis develops early after hypoxic-dysmetabolic insult to the neonatal rat spinal cord in vitro. Neuroscience 169:325-338.

Lee MG, Choi JY, Luo X, Strickland E, Thomas PJ, Muallem S (1999) Cystic fibrosis transmembrane conductance regulator regulates luminal Cl^-/HCO_3^- exchange in mouse submandibular and pancreatic ducts. J Biol Chem 274:14670-14677.

Liu GJ, Kalous A, Werry EL, Bennett MR (2006) Purine release from spinal cord microglia after elevation of calcium by glutamate. Mol Pharmacol 70:851-859.

Livak KJ, Schmittgen TD (2001) Analysis of relative gene expression data using real-time quantitative PCR and the $2^{-\Delta\Delta C}{}_T$ Method. Methods 25:402-408.

Lüscher HR, Larkum ME (1998) Modeling action potential initiation and back-propagation in dendrites of cultured rat motoneurons. J Neurophysiol 80:715-729.

Marchetti C, Pagnotta S, Donato R, Nistri A (2002) Inhibition of spinal or hypoglossal motoneurons of the newborn rat by glycine or GABA. Eur J Neurosci 15:975-983.

McLennan, H (1970) Synaptic Transmission. 2nd edition. W. B. Saunders & Co.

McNicholas CM, Guggino WB, Schwiebert EM, Hebert SC, Giebisch G, Egan ME (1996) Sensitivity of a renal K^+ channel (ROMK2) to the inhibitory sulfonylurea compound glibenclamide is enhanced by coexpression with the ATP-binding cassette transporter cystic fibrosis transmembrane regulator. Proc Natl Acad Sci U S A 93:8083-8088.

Mikawa S, Wang C, Shu F, Wang T, Fukuda A, Sato K (2002) Developmental changes in KCC1, KCC2 and NKCC1 mRNAs in the rat cerebellum. Brain Res Dev Brain Res 136:93-100.

Mironov SL, Langohr K, Haller M, Richter DW (1998) Hypoxia activates ATP-dependent potassium channels in inspiratory neurones of neonatal mice. J Physiol 509:755-766.

Molander C, Xu Q, Grant G (1984) The cytoarchitectonic organization of the spinal cord in the rat. I. The lower thoracic and lumbosacral cord. J Comp Neurol 230:133-141.

Mulberg AE, Resta LP, Wiedner EB, Altschuler SM, Jefferson DM, Broussard DL (1995) Expression and localization of the cystic fibrosis transmembrane conductance regulator mRNA and its protein in rat brain. J Clin Invest 96:646-652.

Mulberg AE, Weyler RT, Altschuler SM, Hyde TM (1998) Cystic fibrosis transmembrane conductance regulator expression in human hypothalamus. Neuroreport 9:141-144.

Mulberg AE, Wiedner EB, Bao X, Marshall J, Jefferson DM, Altschuler SM (1994) Cystic fibrosis transmembrane conductance regulator protein expression in brain. Neuroreport 5:1684–1688.

Müller F, Heinke B, Sandkühler J (2003) Reduction of glycine receptor-mediated miniature inhibitory postsynaptic currents in rat spinal lamina I neurons after peripheral inflammation. Neuroscience 122:799-805.

Nishimaru H, Iizuka M, Ozaki S, Kudo N (1996) Spontaneous motoneuronal activity mediated by glycine and GABA in the spinal cord of rat fetuses in vitro. J Physiol 497:131-143.

Nishimaru H, Kakizaki M (2009) The role of inhibitory neurotransmission in locomotor circuits of the developing mammalian spinal cord. Acta Physiol 197:83-97.

Niu N, Zhang J, Guo Y, Yang C, Gu J (2009) Cystic fibrosis transmembrane conductance regulator expression in human spinal and sympathetic ganglia. Lab Invest 89:636-644.

Nuñez JL, McCarthy MM (2007) Evidence for an extended duration of GABA-mediated excitation in the developing male versus female hippocampus. Dev Neurobiol 67:1879-1890.

O'Donnell ME, Martinez A, Sun D (1995) Cerebral microvascular endothelial cell Na-K-Cl cotransport: regulation by astrocyte-conditioned medium. Am J Physiol 268:C747-C754.

O'Mahony MS, FitzGerald MX (1991) Cystic fibrosis and seizures. Lancet 338:259.

Ostroumov K (2007) A new stochastic tridimensional model of neonatal rat spinal motoneuron for investigating compartmentalization of neuronal conductances and their influence on firing. J Neurosci Methods 163:362-372.

Ostroumov K, Grandolfo M, Nistri A (2007) The effects induced by the sulphonylurea glibenclamide on the neonatal rat spinal cord indicate a novel mechanism to control neuronal excitability and inhibitory neurotransmission. Br J Pharmacol 150:47–57.

Painter RG, Valentine VG, Lanson NA Jr, Leidal K, Zhang Q, Lombard G, Thompson C, Viswanathan A, Nauseef WM, Wang G, Wang G (2006) CFTR Expression in human neutrophils and the phagolysosomal chlorination defect in cystic fibrosis. Biochemistry 45:10260–10269.

Payne JA, Rivera C, Voipio J, Kaila K (2003) Cation-chloride co-transporters in neuronal communication, development and trauma. Trends Neurosci 26:199-206.

Payne JA, Stevenson TJ, Donaldson LF (1996) Molecular characterization of a putative K-Cl cotransporter in rat brain. A neuronal-specific isoform. J Biol Chem 271:16245-16252.

Perrin FE, Boisset G, Lathuilière A, Kato AC (2006) Cell death pathways differ in several mouse models with motoneurone disease: analysis of pure motoneurone populations at a presymptomatic age. J Neurochem 98:1959-1972.

Perrot-Sinal TS, Sinal CJ, Reader JC, Speert DB, McCarthy MM (2007) Sex differences in the chloride cotransporters, NKCC1 and KCC2, in the developing hypothalamus. J Neuroendocrinol 19:302-308.

Plotkin MD, Kaplan MR, Peterson LN, Gullans SR, Hebert SC, Delpire E (1997a) Expression of the Na^+-K^+-$2Cl^-$ cotransporter BSC2 in the nervous system. Am J Physiol 272:C173-C183.

Plotkin MD, Snyder EY, Hebert SC, Delpire E (1997b) Expression of the Na-K-2Cl cotransporter is developmentally regulated in postnatal rat brains: a possible mechanism underlying GABA's excitatory role in immature brain. J Neurobiol 33:781-795.

Pond BB, Berglund K, Kuner T, Feng G, Augustine GJ, Schwartz-Bloom RD (2006) The chloride transporter Na^+-K^+-Cl^- cotransporter isoform-1 contributes to intracellular chloride increases after in vitro ischemia. J Neurosci 26:1396-1406.

Price TJ, Cervero F, de Koninck Y (2005) Role of cation-chloride-cotransporters (CCC) in pain and hyperalgesia. Curr Top Med Chem 5:547-555.

Quattrucci S, Rolla M, Cimino G, Bertasi S, Cingolani S, Scalercio F, Venuta F, Midulla F (2005) Lung transplantation for cystic fibrosis: 6-year follow-up. J Cyst Fibros 4:107-114.

Reddy MM, Quinton PM, Haws C, Wine JJ, Grygorczyk R, Tabcharani JA, Hanrahan JW, Gunderson KL, Kopito RR (1996) Failure of the cystic fibrosis transmembrane conductance regulator to conduct ATP. Science 271:1876-1879.

Reisin IL, Prat AG, Abraham EH, Amara JF, Gregory RJ, Ausiello DA, Cantiello HF (1994) The cystic fibrosis transmembrane conductance regulator is a dual ATP and chloride channel. J Biol Chem 269:20584-20591.

Rheims S, Holmgren CD, Chazal G, Mulder J, Harkany T, Zilberter T, Zilberter Y (2009) GABA action in immature neocortical neurons directly depends on the availability of ketone bodies. J Neurochem 110:1330-1338.

Riordan JR (2008) CFTR function and prospects for therapy. Annu Rev Biochem 77:701-726.

Riordan JR, Rommens JM, Kerem B, Alon N, Rozmahel R, Grzelczak Z, Zielenski J, Lok S, Plavsic N, Chou JL, et al (1989) Identification of the cystic fibrosis gene: cloning and characterization of complementary DNA. Science 245: 1066-1073.

Rivera C, Voipio J, Payne JA, Ruusuvuori E, Lahtinen H, Lamsa K, Pirvola U, Saarma M, Kaila K (1999) The K^+/Cl^- co-transporter KCC2 renders GABA hyperpolarizing during neuronal maturation. Nature 397:251-255.

Russell JM (2000) Sodium-potassium-chloride cotransport. Physiol Rev 80:211-276.

Safronov BV, Wolff M, Vogel W (2000) Excitability of the soma in central nervous system neurons. Biophys J 78:2998-3010.

Schultz BD, Singh AK, Devor DC, Bridges RJ (1999) Pharmacology of CFTR chloride channel activity. Physiol Rev 79:109-144.

Segev, I. (1998) Cable and Compartmental Models of Dendritic Trees. In: J. M. Bower and D. Beeman (eds.). *The Book of GENESIS: Exploring realistic neural models with the GEneral NEural SImulation System (2nd edition).* Telos, Springer-Verlag New York. 149-168.

Sernagor E, Chabrol F, Bony G, Cancedda L (2010) GABAergic control of neurite outgrowth and remodeling during development and adult neurogenesis: general rules and differences in diverse systems. Front Cell Neurosci 4:11.

Sheppard DN, Robinson KA (1997) Mechanism of glibenclamide inhibition of cystic fibrosis transmembrane conductance regulator Cl^- channels expressed in a murine cell line. J Physiol 503:333-346.

Sheppard DN, Welsh MJ (1999) Structure and function of the CFTR chloride channel. Physiol Rev 79:S23-S45.

Shumaker H, Soleimani M (1999) CFTR upregulates the expression of the basolateral Na^+-K^+-Cl^- cotransporter in cultured pancreatic duct cells. Am J Physiol 277:1100–1110.

Stein V, Hermans-Borgmeyer I, Jentsch TJ, Hübner CA (2004) Expression of the KCl cotransporter KCC2 parallels neuronal maturation and the emergence of low intracellular chloride. J Comp Neurol 468:57-64.

Stein V, Nicoll RA (2003) GABA generates excitement. Neuron 37:375-378.

Stil A, Liabeuf S, Jean-Xavier C, Brocard C, Viemari JC, Vinay L (2009) Developmental up-regulation of the potassium-chloride cotransporter type 2 in the rat lumbar spinal cord. Neuroscience 164:809-21.

Stutts MJ, Canessa CM, Olsen JC, Hamrick M, Cohn JA, Rossier BC, Boucher RC (1995) CFTR as a cAMP-dependent regulator of sodium channels. Science 269:847-850.

Stutts MJ, Rossier BC, Boucher RC (1997) Cystic fibrosis transmembrane conductance regulator inverts protein kinase A-mediated regulation of epithelial sodium channel single channel kinetics. J Biol Chem 272:14037-14040.

Sun D, Murali SG (1999) Na^+-K^+-$2Cl^-$ cotransporter in immature cortical neurons: A role in intracellular Cl^- regulation. J Neurophysiol 81:1939-1948.

Tabcharani JA, Rommens JM, Hou YX, Chang XB, Tsui LC, Riordan JR, Hanrahan JW (1993) Multi-ion pore behaviour in the CFTR chloride channel. Nature 366:79-82.

Takahashi T (1984) Inhibitory miniature synaptic potentials in rat motoneurons. Proc R Soc Lond B Biol Sci 221:103-109.

Thurbon D, Luscher HR, Hofstetter T, Redman SJ (1998) Passive electrical properties of ventral horn neurons in rat spinal cord slices. J Neurophysiol 80:2485-2502.

Uvarov P, Ludwig A, Markkanen M, Pruunsild P, Kaila K, Delpire E, Timmusk T, Rivera C, Airaksinen MS (2007) A novel N-terminal isoform of the neuron-specific K-Cl cotransporter KCC2. J Biol Chem 282:30570-30576.

Vandebrouck C, Melin P, Norez C, Robert R, Guibert C, Mettey Y, Becq F (2006) Evidence that CFTR is expressed in rat tracheal smooth muscle cells and contributes to bronchodilation. Respir Res 7:113.

van den Pol AN, Obrietan K, Chen G (1996) Excitatory actions of GABA after neuronal trauma. J Neurosci 16:4283-4292.

Vu TQ, Payne JA, Copenhagen DR (2000) Localization and developmental expression patterns of the neuronal K-Cl cotransporter (KCC2) in the rat retina. J Neurosci 20:1414-1423.

Wang C, Shimizu-Okabe C, Watanabe K, Okabe A, Matsuzaki H, Ogawa T, Mori N, Fukuda A, Sato K (2002) Developmental changes in KCC1, KCC2, and NKCC1 mRNA expressions in the rat brain. Brain Res Dev Brain Res 139:59-66.

Wang DD, Bordey A (2008) The astrocyte odyssey. Prog Neurobiol 86:342-367.

Weyler RT, Yurko-Mauro KA, Rubenstein R, Kollen WJ, Reenstra W, Altschuler SM, Egan M, Mulberg AE (1999) CFTR is functionally active in GnRH-expressing GT1-7 hypothalamic neurons. Am J Physiol 277:C563-C571.

Williams JR, Sharp JW, Kumari VG, Wilson M, Payne JA (1999) The neuron-specific K-Cl cotransporter, KCC2. Antibody development and initial characterization of the protein. J Biol Chem 274:12656-12664.

Wongmongkolrit T, Wyszynski R, Hershey CO, Varnes AW (1985) Evidence of subclinical extrapyramidal hemosiderosis in cystic fibrosis. Acta Neuropathol 65:265-269.

Wu WL, Ziskind-Conhaim L, Sweet MA (1992) Early development of glycine- and GABA-mediated synapses in rat spinal cord. J Neurosci 12:3935–3945.

Yamada J, Okabe A, Toyoda H, Kilb W, Luhmann HJ, Fukuda A (2004) Cl^- uptake promoting depolarizing GABA actions in immature rat neocortical neurones is mediated by NKCC1. J Physiol 557:829-841.

Zhang LL, Delpire E, Vardi N (2007) NKCC1 does not accumulate chloride in developing retinal neurons. J Neurophysiol 98:266-277.

Ziskind-Conhaim L (1998) Physiological functions of GABA-induced depolarizations in the developing rat spinal cord. Perspect Dev Neurobiol 5:279-287.